

On Fast Attitude Filtering Based on Matrix Fisher Distribution with Stability Guarantee

Shijie Wang, Haichao Gui, and Rui Zhong

Abstract—This paper addresses two interrelated problems of the nonlinear filtering mechanism and fast attitude filtering with the matrix Fisher distribution (MFD) on the special orthogonal group. By analyzing the distribution evolution along Bayes' rule, we reveal two essential properties that enhance the performance of Bayesian attitude filters with MFDs, particularly in challenging conditions, from a theoretical viewpoint. Benefiting from the new understanding of the filtering mechanism associated with MFDs, two closed-form filters with MFDs is then proposed. These filters avoid the burdensome computations in previous MFD-based filters by introducing linearized error systems with right-invariant errors but retaining the two advantageous properties. Moreover, we leverage the two properties and closed-form filtering iteration to prove the almost-global exponential stability of the proposed filter with right-invariant error for the single-axis rotation, which, to our knowledge, is not achieved by existing directional statistics-based filters. Numerical simulations demonstrate that the proposed filters are significantly more accurate than the classic invariant Kalman filter. Besides, they are also as accurate as recent MFD-based Bayesian filters in challenging circumstances with large initial error and measurement uncertainty but consumes far less computation time (about 1/5 to 1/100 of previous MFD-based attitude filters).

Index Terms—Bayesian filters, attitude estimation, matrix Fisher distribution, nonlinear filtering, special orthogonal group

I. INTRODUCTION

THE problem of attitude estimation with uncertain noisy measurements is a core task in the navigation of mobile robotics, aeronautics, astronautics, and other realms. In these realms, many systems, such as unmanned aerial vehicles and nanosatellites, have limited computational resources and low-cost sensors. Meanwhile, the unique fact that attitude evolves on the special orthogonal group $SO(3)$, makes it difficult for attitude estimators to accurately handle large errors and uncertainties with low computational complexity. As a result, it is valuable and challenging to design efficient attitude estimators on $SO(3)$ with limits of computational resources.

This work was supported in part by the National Natural Science Foundation of China under Grant 12422214.

Shijie Wang is with School of Astronautics, Shenyuan Honors College, Beihang University, Beijing, 100191, China (e-mail: wangsj2001@buaa.edu.cn).

Haichao Gui is with School of Astronautics and the MOE Key Laboratory of Spacecraft Design, Optimization and Dynamic Simulation, Beihang University, Beijing, 100191, China (e-mail: hcgui@buaa.edu.cn, corresponding author).

Rui Zhong is with School of Astronautics, Beihang University, Beijing, 100191, China (e-mail: zhongruia@163.com).

Attitude observers, as deterministic approaches, are designed directly on $SO(3)$, avoiding singularities of local coordinates and achieving theoretical guarantees of stability and convergence speed. In [1], non-linear complementary filters were proposed and proved to be almost globally stable with the Lyapunov analysis. Higher-order nonlinear complementary filters were proposed in [2] for estimation on Lie group. More recently, hybrid observers were designed for attitude estimation, providing stronger forms of stability, such as global asymptotic stability [3] and global exponential stability [4]. The hybrid observers were further developed for simultaneously estimating attitude and gyro bias with global exponential stability [5], pose estimation using landmark measurements [6], attitude estimation using intermittent and multirate vector measurements [7], etc. A notable advantage of these deterministic observer approaches is that they admit rigorous Lyapunov-based proofs of stability and convergence rates, which makes them highly reliable and theoretically sound. Instead of deterministic observers, this paper focuses on stochastic estimation techniques. These techniques take stochastic properties into account and describe state uncertainty in terms of probability density, as introduced follows

For attitude estimation, the classic multiplicative extended Kalman filter (MEKF) was developed in [8] and [9], representing attitude by quaternion and uncertainty distribution around the mean attitude by a Gaussian distribution on the three-dimensional Euclidean space. More recently, the invariant extended Kalman filter (IEKF) was developed in [10]–[15] by utilizing more geometric and algebraic properties of Lie groups and was applied to estimate attitude for spacecraft navigation, [16], SLAM [17]–[19] and other industrial applications. In the IEKF, the Gaussian distributions in exponential coordinates (a coordinate system with the exponential map near the group identity [20]) are used to represent the uncertainty of states [21] and the linearized error system is adopted to propagate uncertainty. Another Gaussian distribution in exponential coordinates, referred to as the concentrated Gaussian distribution (CGD) [22]–[24] is also used to represent the uncertainty of states and to construct Kalman filters (KF) on Lie groups, such as CD-LR-EKF [25]. When applying these two distributions to derive variants of the EKF, the resultant filtering gain tuning and covariance update still depend on the linearized error system and the properties of Gaussian distributions on the n -dimensional Euclidean space, which remain the same as the KF. This implies that the state error is still treated as a random variant following Gaussian distributions. This strategy is effective for systems

with sufficient *a priori* information and small measurement errors but limits the performance of the IEKF and other similar filters in challenging circumstances with large initial errors and measurement uncertainties. For example, it is difficult for the Gaussian distribution in local coordinates to characterize the attitude with high uncertainty due to wrapped errors [26].

To address the shortcomings brought by the structure of filters with Gaussian distributions in the Euclidean space, the robotics community has increasingly recognized the importance of properly defining distributions on Lie groups [21]. A series of notable approaches to construct filters with distributions on $SO(3)$ are assumed density filters with directional statistics, a branch of statistics dealing with observations lying on the nonlinear manifold [27]–[29]. The assumed density filters for attitude estimation make use of the structure of Bayesian filters and the distributions provided by directional statistics to approximate the underlying posterior distribution of attitude, such as the matrix Fisher distribution (MFD) on Stiefel manifolds [30], [31] and the Bingham distribution on the n -dimensional sphere [32]. In [33], Bayesian attitude filters were designed with MFDs on $SO(3)$, using the first moment to propagate distributions along the kinematics. Meanwhile, several attitude filters have been constructed based on Bingham distributions on the three-dimensional sphere [34], [35]. Recently, attitude filters were proposed with a newly defined matrix Fisher-Gaussian distribution on $SO(3) \times \mathbb{R}^n$ in [36] and [26], with methodologies similar to those in [33].

A range of assumed density filters with the MFDs demonstrate superiorities compared to the classic MEKF in challenging circumstances but have computational burdens that far exceed the MEKF. Although approximate solutions were presented in [37] to accelerate computations, these filters still spend much more computation time than variants of the EKF, as shown in Section VI. Furthermore, the reason why filters with MFDs perform better than variations of the EKF such as the MEKF in challenging circumstances, still needs more in-depth investigations. In [26], it was intuitively attributed to the reasons that these works do not use linearization to construct estimators and avoid the wrapped errors caused by Gaussian distributions on local coordinates. There is, however, a lack of comprehensive theoretical explanations on how wrapped errors affect attitude estimation and why the uncertainties in attitude estimation are increased by the MFD-based estimator when initial errors are large and the initial confidence is falsely high, as observed in [33], [36]. What mechanisms make the MFD-based filters perform better and how to design fast MFD-based filters are two closely interrelated problems. Once the crucial properties associated with the advantageous performance of MFD-based filters are identified mathematically, new filters can be designed by preserving these properties and streamlining the rest for faster computations.

In this paper, we reveal two properties intrinsic in MFDs that improve the performance of MFD-based attitude filters, and then propose two fast MFD-based filters. The proposed filters retain the two properties while introducing linearized error systems to significantly enhance computational speed. As a result, they are almost as accurate as previous MFD-based attitude filters but consume far less computational time. The

proposed filter with right-invariant error is also endowed with almost-global exponential stability guarantee for the estimation of the single-axis rotation. To the best of our knowledge, there are no results in the literature about estimators with directional statistics achieving any stability properties. The detailed methodologies and contributions are summarized as follows.

In Section III, the evolution of the distribution on $SO(3)$ along Bayes' rule is studied, which indicates how the statistical characteristics of the prior and the likelihood distributions impact the posterior distribution. To further characterize the distribution on $SO(3)$, we define two new parameters for both MFDs and CGDs, which are referred to as the mean angle and concentration parameter respectively. The nonlinear recurrence relation of the two parameters describe how the differences in mean attitudes affect the posterior distribution. By comparing their expressions for the posterior distribution derived from the Bayesian filter with MFDs and CGDs, two key properties of the MFD-based Bayesian filter are identified mathematically:

- Due to the special correlation of the two parameters, the difference in the mean attitudes of the prior and the likelihood distributions raises the uncertainty of the posterior distribution for rotations around a specific axis.
- Because of the nonlinear recurrence relations of the parameters, the mean angle of the posterior distribution from the filter with MFDs is always closer to a higher-confidence mean angle (between the likelihood and the prior distributions) than that from the filter with CGDs.

The above properties enable MFD-based filters to adjust the uncertainty in the attitude estimation and to filter out wrong information with low confidence much faster.

These two properties are intrinsic to MFDs and independent of the accuracy of the method used to approximate the underlying prior and likelihood distributions (such as the first-moment matching or the unscented transformation). Thus, in Section IV, we construct two fast nonlinear filters with MFDs on $SO(3)$, which utilize linearization to approximate the prior and the likelihood distributions but retain the two key properties. We establish two probability models with left- and right-invariant errors respectively to represent the uncertainty of attitude, and both two invariant errors are characterized by MFDs, instead of Gaussian distributions in exponential coordinates as adopted by the IEKF. In the filtering procedure, the parameters of MFDs are calculated through linearized error equations to approximate the underlying prior and likelihood distributions with first-order precision. Then the prior and the likelihood distributions approximated by MFDs are fused with Bayes' rule to obtain the posterior distribution on $SO(3)$. Due to the new understanding of the properties of Bayesian filters with MFDs, the two filters retain the key factors enabling higher estimation accuracy while avoiding solving nonlinear equations, as required by previous MFD-based estimators [33], for uncertainty propagation, which significantly reduces the computational complexity of the proposed filters. Then, the stability properties of the proposed filter with right-invariant error as an observer are studied in Section ???. The one-dimensional form of the proposed filter is derived for

a deterministic single-axis rotation case, leading to almost-global exponential stability, i.e., the estimation error converges exponentially to zero for all initial conditions except from a set of Lebesgue measure zero.

In challenging circumstances with large initial error and measurement uncertainty, numerical simulations presented in Section VI illustrate that the two proposed filters exhibit almost identical accuracy as filter in [33] and perform even better in dealing with non-isotropic vector measurement noise. Simulation results also indicate that the proposed filters are more accurate than the well-established IEKF, which outperforms many variants of the EKF in state estimation on Lie groups [11], [12], [15]. Moreover, the proposed filters only spend $1/5 \sim 1/100$ of the previous MFD-based attitude filters in [33] and [37]. The conclusion is drawn in Section VII.

II. PRELIMINARIES

A. Notations and Some Facts

Throughout this paper, \mathbb{R}^n denotes the n -dimensional Euclidean space, and I_n denotes the $n \times n$ identity matrix. Consider a rigid body with its body-fixed frame $\mathcal{F}_B = \{b_1, b_2, b_3\}$, where the vector $b_i \in \mathbb{R}^3$ is the i -th basis of \mathcal{F}_B . Similarly, we define an inertial frame and its basis $\mathcal{F}_I = \{e_1, e_2, e_3\}$. Then the attitude of the rigid body is the orientation of \mathcal{F}_B relative to \mathcal{F}_I , which can be represented by a rotation matrix $R \in \mathbb{R}^{3 \times 3}$ given by $R_{ij} = e_i \cdot b_j$, where R_{ij} is the element of the i -th row and j -th column of R . When both \mathcal{F}_B and \mathcal{F}_I are right-handed orthonormal frames, the rotation matrices with matrix multiplication form the special orthogonal group

$$SO(3) = \{R \in \mathbb{R}^{3 \times 3} | R^T R = I_3, \det[R] = 1\},$$

where $\det[\cdot]$ gives the determinant of a matrix. The tangent space at $R \in SO(3)$ is denoted by $T_R SO(3)$. The Lie algebra of $SO(3)$ is denoted by $\mathfrak{so}(3) = \{X \in \mathbb{R}^{3 \times 3} | X = -X^T\}$, and the map: $\wedge : \mathbb{R}^3 \rightarrow \mathfrak{so}(3)$ is an isometry between $\mathfrak{so}(3)$ and \mathbb{R}^3 . The hat map is defined such that $x^\wedge y = x \times y$ for any $x, y \in \mathbb{R}^3$, and its inverse map is denoted by \vee .

The notations \tilde{a} and \hat{a} denote a measured variable and an estimated variable respectively. The subscript k denotes the k -th time-step of the time sequence $\{t_0, t_1, \dots\}$ and the superscript i denotes the i -th term of the set $\{a^1, a^2, \dots\}$. The trace of a matrix is denoted by $\text{tr}(\cdot)$, and the function $e^{\text{tr}(\cdot)}$ is abbreviated as $\text{etr}(\cdot)$. The sign function is denoted by $\text{sign}(\cdot)$. The Frobenius norm of a matrix $M \in \mathbb{R}^{3 \times 3}$ is defined as $\|M\|_F = \sqrt{\text{tr}(M^T M)}$.

The following equations involving the map \wedge and trace will be repeatedly used. For any $A \in \mathbb{R}^{3 \times 3}$, $R \in SO(3)$, and $a, b \in \mathbb{R}^3$, we have

$$(Ra)^\wedge = Ra^\wedge R^T \quad (1)$$

$$(a^\wedge A + A^T a^\wedge) = [(\text{tr}(A) I_3 - A) a]^\wedge, \quad (2)$$

$$(ba^T - ab^T)^\vee = a^\wedge b. \quad (3)$$

B. Distributions on $SO(3)$

1) *The matrix Fisher distribution*: The MFD is a compact exponential density on the Stiefel manifold. In recent years, the

MFD has been applied to $SO(3)$ to represent the uncertainty of attitude, which was introduced initially in [33]. The probability density function (PDF) of a random rotation matrix $R \sim \mathcal{M}(F)$ is defined as

$$p(R \in SO(3); F) = \frac{1}{c(F)} \text{etr}[F^T R], \quad (4)$$

where $F \in \mathbb{R}^{3 \times 3}$ is a parameter and $c(F) \in \mathbb{R}$ is the normalized constant. $c(F)$ is calculated by $c(F) = \int_{SO(3)} \text{etr}[F^T R] dR$, where dR is the bi-invariant Haar measure. The parameter F can be decomposed via the proper singular value decomposition (SVD) [38] as follows

$$F = USV^T, \quad (5)$$

where $U, V \in SO(3)$ and $S = \text{diag}[s_1, s_2, s_3] \in \mathbb{R}^{3 \times 3}$ with $s_1 \geq s_2 \geq |s_3| \geq 0$. Given a random rotation matrix $R \sim \mathcal{M}(F)$, the *mean attitude* of R is defined as the attitude that maximizes the density function and minimizes the Frobenius mean squared error, given by $M = UV^T \in SO(3)$.

The i -th principal axis of the MFD is studied in [33], which is Ue_i when resolved in \mathcal{F}_I , or Ve_i when resolved in \mathcal{F}_B . The parameter $s_j + s_k$ illustrates the concentration of dispersion relative to the i -th principal axis. We can also apply the proper right polar decomposition to F , which gives

$$F = MK, \quad (6)$$

where $M \in SO(3)$ is called the polar component and $K \in \mathbb{R}^{3 \times 3}$ is a symmetric positive-definite matrix referred to as the elliptical component. Compared with (5), it follows that $M = UV^T$ and $K = VSV^T$, which represent the center of the distribution, and the dispersion relative to the mean attitude, respectively. Similarly, the proper left polar decomposition of F is given by

$$F = K' M', \quad (7)$$

where $K' = USU^T$ and $M' = UV^T$.

Next, we present the transformation of MFDs under rotation and transpose.

Lemma II.1. *Given fixed matrices $R_l, R_r \in SO(3)$, and $R \sim \mathcal{M}(F)$, the random rotation matrix $R' = R_l R R_r \in SO(3)$ follows a MFD on $SO(3)$ with*

$$R' \sim \mathcal{M}(R_l F R_r). \quad (8)$$

Proof. Since dR is the bi-invariant Haar measure, we can derive

$$\begin{aligned} p(R') &\propto \text{etr}(F^T R) = \text{etr}(F^T R_l^T R' R_r^T) \\ &= \text{etr}((R_l F R_r)^T R'), \end{aligned}$$

which shows (8). \square

Proposition II.1. *Suppose that $R \sim \mathcal{M}(N)$ and $N \in \mathbb{R}^{3 \times 3}$ is a symmetric matrix. The random rotation matrix $R_T = R^T$ is characterized by the following probability,*

$$p(R_T) = \frac{1}{c(N)} \text{etr}(N R_T), \quad (9)$$

i.e., $R_T \sim \mathcal{M}(N)$ as well.

Proof. Using the Jacobian matrix $\partial R/\partial R_T = I_3$, the density of R_T is

$$p(R_T) \propto \text{etr}(N^T R) = \text{etr}(R_T N) = \text{etr}(N R_T),$$

which shows (9). \square

2) *The concentrated Gaussian distribution:* The CGD [22]–[25] is a generalization of the Gaussian distribution on Lie groups. Following [24], the PDF of a random rotation matrix R following CGD is defined as

$$p(R \in SO(3); M, P) = \frac{1}{c} \exp \left\{ -\frac{1}{2} \left[\log(M^T R)^\vee \right]^T (P)^{-1} \left[\log(M^T R)^\vee \right] \right\}, \quad (10a)$$

or

$$p(R \in SO(3); M, P) = \frac{1}{c} \exp \left\{ -\frac{1}{2} \left[\log(RM^T)^\vee \right]^T (P)^{-1} \left[\log(RM^T)^\vee \right] \right\}, \quad (10b)$$

where c is the normalized constant, $M \in SO(3)$ is the mean attitude and $P \in \mathbb{R}^{3 \times 3}$ is a symmetric matrix. The rotation matrices following (10a) or (10b) are denoted by $R \sim \mathcal{N}_L(M, P)$ or $R \sim \mathcal{N}_R(M, P)$.

C. System Models

Let $R \in SO(3)$ represent the attitude of a rigid body with respect to \mathcal{F}_I . The continuous attitude kinematics without noise in terms of rotation matrix is written as

$$R_t^T dR_t = \omega_t dt, \quad (11)$$

where $\omega_t \in \mathbb{R}^3$ is the angular velocity relative to \mathcal{F}_I expressed in \mathcal{F}_B . In practical attitude estimation tasks, the angular velocity is often measured by rate gyroscopes, and its typical measurement model without bias is given by

$$\tilde{\omega}_t = \omega_t - H dW, \quad (12)$$

where dW is a 3-dimensional Wiener process and $H \in \mathbb{R}^{3 \times 3}$ describes the magnitude of noise. The kinematics (11) and (12) can be discretized with time sequence $\{t_0, t_1, \dots, t_k, \dots\}$ and the fixed time step $h = t_k - t_{k-1}$ as

$$R_k = R_{k-1} \exp \{ (h\tilde{\omega}_k + w_k)^\wedge \}, \quad (13)$$

where $w_k = H_k \Delta W$ is a centered Gaussian with a covariance matrix $Q_k = h H_k H_k^T$. Additionally, vector measurements are usually used to correct the accumulation error of gyros, and the corresponding measurement model is given by

$$\tilde{b}_k^i = R_k^T e_k^i + v_k^i, i = 1, 2, \dots, n \quad (14)$$

where $e_k^i \in \mathbb{R}^3$ is a known vector expressed in \mathcal{F}_I , \tilde{b}_k^i is the corresponding measurement expressed in \mathcal{F}_B and v_k^i is a centered Gaussian noise with a covariance matrix G_k^i .

III. NONLINEAR FILTERING MECHANISM CAUSED BY MFDs

In this section, we analyze the evolution of the distribution on $SO(3)$ along Bayes' rule, which leads to the differences in the filtering mechanism between MFD-based Bayesian filters and CGD-based Bayesian filters.

A. Distributions on the subset of $SO(3)$

We focus on a special subset containing the mean attitudes of both the prior and the likelihood distributions, rather than the entire $SO(3)$, such that how the difference in mean attitudes of the prior and the likelihood distributions influences the posterior distribution are highlighted. The following defines a subset generated by the mean attitude rotating around a specific axis.

Definition III.1. Consider a deterministic attitude represented by M . The subset of $SO(3)$ generated by M rotating around a specific axis w_0 is denoted by $\mathcal{S}_M(w_0)$, which is defined as

$$\mathcal{S}_M(w_0) \triangleq \{R(\theta) \in SO(3) | R(\theta) = M \exp(\theta \omega_0^\wedge), \theta \in [-\pi, \pi)\}. \quad (15)$$

Proposition III.1. Consider any two rotation matrices $M_1, M_2 \in SO(3)$. There always exists a subset $\mathcal{S}_{M_0}(w_0)$ such that $M_1, M_2 \in \mathcal{S}_{M_0}(w_0)$, where M_0 and w_0 are given by

$$M_0 = M_1, w_0 = \frac{\log(M_1^T M_2)^\vee}{\|\log(M_1^T M_2)^\vee\|}$$

Proof. Substituting $\theta = \|\log(M_1^T M_2)^\vee\|$ into (16), we have

$$R(\theta) = M_1 \exp(\log(M_1^T M_2)) = M_2,$$

which indicates $M_2 \in \mathcal{S}_{M_0}(w_0)$. \square

Definition III.1 and Proposition III.1 can be viewed as an equivalence of Euler's rotation theorem. The proposition implies that the mean attitudes of any two distributions can be included in the same subset. Besides, the difference between the mean attitudes of two distributions, such as the prior and the likelihood distributions, can be represented by a one-dimensional scalar θ .

Then, the probability density functions of both MFDs and CGDs on the subset defined by Definition III.1 are each proven to be single variable functions of θ with two parameters.

Theorem III.1. Consider a random attitude $R \sim \mathcal{M}(F)$ and the proper right polar decomposition of F is given by $F = MK$. Let $\mathcal{S}_{M_0}(w_0)$ be a subset of $SO(3)$ defined as (15). If the mean attitude M belongs to $\mathcal{S}_{M_0}(w_0)$, the probability density of the elements in $\mathcal{S}_{M_0}(w_0)$ can be rewritten as

$$p(R(\theta)) \propto \exp \left[(\text{tr}(K) - w_0^T K w_0) \cos(\theta - \bar{\theta}) \right], \quad (16)$$

where $\bar{\theta} = w_0 \cdot \log(M_0 M^T)^\vee$.

Proof. Because $M \in \mathcal{S}_{M_0}(w_0)$, we have $M = M_0 \exp(\bar{\theta} \omega_0^\wedge)$. Then every R belonging to $\mathcal{S}_{M_0}(w_0)$ can be rewritten as

$$R(\theta) = M \exp((\theta - \bar{\theta}) \omega_0^\wedge). \quad (17)$$

Substituting (17) into (4) and using Rodrigues' rotation formula [39], we have

$$\begin{aligned}
 p(R(\theta)) &= \frac{1}{c(F)} \text{etr} [KM^T M \exp((\theta - \bar{\theta})\omega_0^\wedge)] \\
 &= \frac{1}{c(F)} \text{etr} [K \cos(\theta - \bar{\theta}) + K\omega_0^\wedge \sin(\theta - \bar{\theta}) \\
 &\quad + K\omega_0\omega_0^T (1 - \cos(\theta - \bar{\theta}))] \\
 &= \frac{1}{c(F)} \exp [\text{tr}(K) \cos(\theta - \bar{\theta}) + 0 + \\
 &\quad \omega_0^T K \omega_0 (1 - \cos(\theta - \bar{\theta}))] \\
 &= \frac{e^{\omega_0^T K \omega_0}}{c(F)} \exp [(\text{tr}(K) - \omega_0^T K \omega_0) \cos(\theta - \bar{\theta})],
 \end{aligned} \tag{18}$$

which gives (16). \square

The PDF on $\mathcal{S}_{M_0}(w_0)$ given by (16) is similar to the von-Mises distribution on \mathbb{S}^2 [40], which is defined as

$$p(\theta) \propto e^{\kappa \cos(\theta - \bar{\theta})}, \tag{19}$$

where the angle parameter $\bar{\theta}$ maximizes the probability $p(\theta)$ and κ describes how the distribution concentrates about $\bar{\theta}$. Compared with (19), we can define two similar parameters to describe the statistical characterization of MFDs on $\mathcal{S}_{M_0}(w_0)$ as follows.

Definition III.2. Consider a random attitude $R \sim \mathcal{M}(F)$. If the probability of elements belonging to $\mathcal{S}_{M_0}(w_0)$ can be rewritten as

$$p(R(\theta)) \propto e^{\kappa \cos(\theta - \bar{\theta})},$$

then $\bar{\theta}$ is referred to as the mean angle of $\mathcal{M}(F)$ on $\mathcal{S}_{M_0}(w_0)$ and κ is referred to as the concentration parameter of $\mathcal{M}(F)$ on $\mathcal{S}_{M_0}(w_0)$.

According to Theorem III.1, the mean angle and concentration parameter of $\mathcal{M}(F)$ on $\mathcal{S}_{M_0}(w_0)$ such that $M \in \mathcal{S}_{M_0}(w_0)$ are given by

$$\bar{\theta} = w_0 \cdot \log(M_0 M^T)^\vee \text{ and } \kappa = \text{tr}(K) - w_0^T K w_0.$$

When w_0 is the i -th principal axis expressed in \mathcal{F}_B , i.e., $w_0 = V e_i$, we have

$$\begin{aligned}
 \kappa &= \text{tr}(K) - w_0^T K w_0 \\
 &= s_i + s_j + s_k - e_i^T V^T V S V^T V e_i = s_j + s_k,
 \end{aligned}$$

where $\{i, j, k\} = \{1, 2, 3\}$. Moreover, if $M_0 = M$, (18) can be rewritten as

$$p(R(\theta)) = \frac{s_i}{c(F)} \exp[(s_j + s_k) \cos(\theta)],$$

which is the same as (42) in [33]. Therefore, Definition III.2 can be viewed as a generalization of the geometric interpretation about MFDs in [33] and the parameters defined in Definition III.2 can describe the dispersion of attitude generated by the mean attitude rotating around any specific axis $w_0 \in \mathbb{S}^2$, instead of merely principal axes.

A similar conclusion can be drawn for CGDs.

Theorem III.2. Consider a random attitude $R \sim \mathcal{N}_L(M, P)$. Let $\mathcal{S}_{M_0}(w_0)$ be a subset of $SO(3)$ defined as (15). If $M \in$

$\mathcal{S}_{M_0}(w_0)$, for $R(\theta) \in \mathcal{S}_{M_0}(w_0)$, the probability density can be rewritten as

$$p(R(\theta)) \propto \exp\left(-\frac{1}{2}(\theta - \bar{\theta})w_0^T P_i^{-1} w_0(\theta - \bar{\theta})\right), \tag{20}$$

where $\bar{\theta} = w_0 \cdot \log(M_0 M^T)^\vee$.

Proof. For $R(\theta) \in \mathcal{S}_{M_0}(w_0)$, we have $R(\theta) = M_0 \exp(\theta \omega_0^\wedge)$. Because M also belongs to $\mathcal{S}_{M_0}(w_0)$, an arbitrary $R(\theta)$ belonging to $\mathcal{S}_{M_0}(w_0)$ can be rewritten as

$$\begin{aligned}
 R(\theta) &= M_0 \exp(\theta \omega_0^\wedge) = M \exp(\bar{\theta} \omega_0^\wedge)^T \exp(\theta \omega_0^\wedge) \\
 &= M \exp((\theta - \bar{\theta}) \omega_0^\wedge).
 \end{aligned} \tag{21}$$

Substituting $R(\theta) = M \exp((\theta - \bar{\theta}) \omega_0^\wedge)$ into the PDF of R , we have

$$p(R(\theta)) \propto \exp\left(-\frac{1}{2}(\theta - \bar{\theta})w_0^T P_i^{-1} w_0(\theta - \bar{\theta})\right),$$

which verifies (20). \square

The density function (20) of CGDs on the subset $\mathcal{S}_{M_0}(w_0)$ is similar to the one-dimensional Gaussian distribution of $\theta \in \mathbb{R}$ with mean $\bar{\theta}$ and variance $w_0^T P_i^{-1} w_0$. Thus the following two parameters are defined to characterize the CGD on $\mathcal{S}_{M_0}(w_0)$.

Definition III.3. Consider a random attitude $R \sim \mathcal{N}_L(M, P)$. If the probability of elements belonging to $\mathcal{S}_{M_0}(w_0)$ can be rewritten as

$$p(R(\theta)) \propto \exp\left[-\frac{(\theta - \bar{\theta})^2}{2\sigma^2}\right], \tag{22}$$

where $R(\theta) \in \mathcal{S}_{M_0}(w_0)$. Then $\bar{\theta}$ is referred to as the mean angle of $\mathcal{N}_L(M, P)$ on $\mathcal{S}_{M_0}(w_0)$ and $1/\sigma^2$ is referred to as the concentration parameter of $\mathcal{N}_L(M, P)$ on $\mathcal{S}_{M_0}(w_0)$.

Remark III.1. Although the two sets of parameters in Definitions III.2 and III.3 are defined via different methods, they have similar statistical meanings and magnitudes. In the density functions (16) and (20), the mean angles maximize the probability density on the subset and the concentration parameters describe how distributions on the subset concentrates about the mean angle. Besides, using Taylor's formula, the density functions (16) can be rewritten as

$$\begin{aligned}
 p(R(\theta)) &\propto \exp[\kappa \cos(\theta - \bar{\theta})] \\
 &\propto \exp\left[-\frac{\kappa(\theta - \bar{\theta})^2}{2} + \mathcal{O}(\|\theta - \bar{\theta}\|^4)\right]
 \end{aligned}$$

which indicates that the two concentration parameters, κ and $1/\sigma^2$, are almost equivalent when the tails of distributions are small. Therefore, the two sets of parameters are comparable.

A numerical example is presented to illustrate these parameters more clearly. Consider a subset $\mathcal{S}_{M_0}(w_0)$ with $M_0 = I_3$ and $w_0 = 1/\sqrt{2} [0, 1, 1]^T$ and three random attitudes characterized by the following MFDs with different parameters of $F_1 = 50I_3$, $F_3 = \exp(\pi/4 \omega_0^\wedge) 50I_3$ and

$$F_2 = \begin{bmatrix} 2 & 0 & 0 \\ 0 & 74 & 72 \\ 0 & 72 & 74 \end{bmatrix},$$

respectively. The traces of F_1 , F_2 , and F_3 are the same, but their mean angles $\bar{\theta}_1$, $\bar{\theta}_2$, $\bar{\theta}_3$ and concentration parameters κ_1 , κ_2 , κ_3 are different. Note that $\kappa_1 = \kappa_3 = 100$, while $\kappa_2 = 4$. Since $\kappa_2 \leq \kappa_1 = \kappa_3$, the distribution $\mathcal{M}(F_2)$ on $\mathcal{S}_{M_0}(w_0)$ is more dispersed than the other two distributions. Besides, $\bar{\theta}_1 = \bar{\theta}_2 = 0$, while $\bar{\theta}_3 = \pi/4$, which implies that the mean angle of $\mathcal{M}(F_3)$ offsets 25° from those of $\mathcal{M}(F_1)$ and $\mathcal{M}(F_2)$. These characteristics are also shown in Fig. 1.

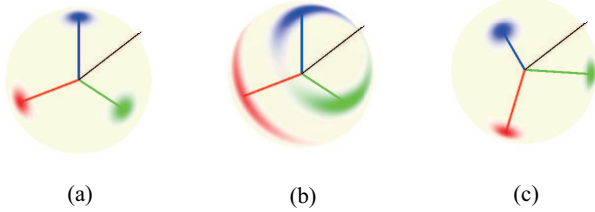


Fig. 1. Matrix Fisher distributions with different parameters. The marginal distribution for each column of R is shown on the unit sphere as red, green and blue shades, as presented in [33]. The red, green and blue lines represent the first, second, and third columns of the mean attitude, respectively, and the black line represents the axis w_0 . (a) $\mathcal{M}(F_1)$: $\kappa_1 = 100$, $\bar{\theta}_1 = 0$; (b) $\mathcal{M}(F_2)$: $\kappa_2 = 4$, $\bar{\theta}_2 = 0$; (c) $\mathcal{M}(F_3)$: $\kappa_3 = 100$, $\bar{\theta}_3 = \pi/4$

B. The evolutions of MFDs and CGDs along Bayes' rule

Next, the evolutions of MFDs and CGDs along Bayes' rule are derived via the evolutions of the characteristic parameters defined in Definitions III.2 and III.3. The evolution of MFDs is given first as follows.

Theorem III.3. *Let the prior attitude distribution be characterized by $R \sim \mathcal{M}(F^-)$ and the likelihood distribution by $M^m|R \sim \mathcal{M}(RK^m)$ with $K^m \in \mathbb{R}^{3 \times 3}$ and $K^m = (K^m)^T$. Denote the proper right polar decomposition of F^- by $F^- = M^-K^-$ and a single sample of $\mathcal{M}(RK^m)$ by \tilde{M}^m . The posterior probability density of $R(\theta) \in \mathcal{S}_{M^-}(w_0)$ can be rewritten as*

$$p(R(\theta)|\tilde{M}^m) \propto \exp[\kappa^+ \cos(\theta - \bar{\theta}^+)], \quad (23)$$

where $\mathcal{S}_{M^-}(w_0)$ containing both M^- and \tilde{M}^m is given by Proposition III.1, and κ^+ and $\bar{\theta}^+$ are given by

$$\kappa^+ = \sqrt{(\kappa^-)^2 + (\kappa^m)^2 + 2\kappa^-\kappa^m \cos(\bar{\theta}^m)}, \quad (24a)$$

$$\bar{\theta}^+ = \text{sign}(\bar{\theta}^m) \arccos\left(\frac{\kappa^- + \kappa^m \cos(\bar{\theta}^m)}{\kappa^+}\right). \quad (24b)$$

In (24a) and (24b), $\bar{\theta}^-$ and $\bar{\theta}^m$ are the mean angles of $\mathcal{M}(F^-)$ and $\mathcal{M}(F^m)$ respectively, and κ^- and κ^m are the concentration parameters of $\mathcal{M}(F^-)$ and $\mathcal{M}(F^m)$ respectively, where $F^m = \tilde{M}^m K^m$. It follows from the definition of $\mathcal{S}_{M^-}(w_0)$ that $\bar{\theta}^- = 0$.

Proof. For $R \in \mathcal{S}_{M^-}(w_0)$, we have $R = M^- \exp(\theta \omega_0^\wedge)$.

Then, using Bayes' rule, we have

$$\begin{aligned} p(R(\theta)|\tilde{M}^m) &\propto p(R)p(M^m = \tilde{M}^m|R) \\ &= \text{etr}((K^-(M^-)^T + K^m(M^m)^T)M^- \exp(\theta \omega_0^\wedge)) \\ &= \text{etr}((K^- + K^m(M^m)^T M^-) \exp(\theta \omega_0^\wedge)). \end{aligned}$$

According to Proposition III.1, $\tilde{M}^m \in \mathcal{S}_{M^-}(w_0)$ and thus we have $(\tilde{M}^m)^T M^- = (\exp(\bar{\theta}^m \omega_0^\wedge))^T$. Therefore, the probability density of the elements belonging to $\mathcal{S}_{M_0}(w_0)$ can be rewritten as

$$\begin{aligned} p(R(\theta)|\tilde{M}^m) &\propto \text{etr}((K^- + K^m(M^m)^T M^-) \exp(\theta \omega_0^\wedge)) \\ &= \text{etr}(K^- \exp(\theta \omega_0^\wedge) + K^m \exp((\theta - \bar{\theta}^m) \omega_0^\wedge)) \\ &\propto \exp[(\text{tr}(K^-) - w_0^T K^- w_0) \cos(\theta) + \\ &\quad (\text{tr}(K^m) - w_0^T K^m w_0) \cos(\theta - \bar{\theta}^m)] \\ &= \exp[(\kappa^- + \kappa^m \cos(\bar{\theta}^m)) \cos(\theta) + \kappa^m \sin(\bar{\theta}^m) \sin(\theta)] \\ &= \exp[\kappa^+ \cos(\theta - \bar{\theta}^+)], \end{aligned}$$

where κ^+ and $\bar{\theta}^+$ are given by the induction formula of the cosine function. This verifies the conclusion. \square

The above theorem indicates how the prior and the likelihood distributions affect the posterior distribution on $\mathcal{S}_{M^-}(w_0)$ when the underlying prior and likelihood distributions are approximated by MFDs. Theorem III.3 can be applied to the filtering procedure of any Bayesian attitude filter using MFDs to represent attitude uncertainty.

A similar theorem is given for the case that the underlying prior and likelihood distributions are approximated by CGDs.

Theorem III.4. *Consider the prior attitude distribution characterized by $R \sim \mathcal{N}_L(M^-, P^-)$ and the likelihood distribution by $M^m|R \sim \mathcal{N}_L(R, P^m)$. Denote a single sample of $\mathcal{N}_L(R, P^m)$ by $\tilde{M}^m \in SO(3)$. The posterior probability density of $R(\theta) \in \mathcal{S}_{M_0}(w_0)$ can be rewritten as*

$$p(R(\theta)|\tilde{M}^m) \propto \exp\left[-\frac{(\theta - \bar{\theta}^+)^2}{2(\sigma^+)^2}\right], \quad (25)$$

The subset $\mathcal{S}_{M^-}(w_0)$ containing M^- and \tilde{M}^m is given by Proposition III.1, and $1/(\sigma^+)^2$ and $\bar{\theta}^+$ are given by

$$\frac{1}{(\sigma^+)^2} = \frac{1}{(\sigma^-)^2} + \frac{1}{(\sigma^m)^2} \quad (26a)$$

$$\bar{\theta}^+ = \frac{(\sigma^-)^2}{(\sigma^m)^2 + (\sigma^-)^2} \bar{\theta}^m. \quad (26b)$$

In (26a) and (26b), $\bar{\theta}^-$ and $\bar{\theta}^m$ are the mean angles of $\mathcal{N}_L(M^-, P^-)$ and $\mathcal{N}_L(\tilde{M}^m, P^m)$ respectively and $1/(\sigma^-)^2$, and $1/(\sigma^m)^2$ are the concentration parameters of $\mathcal{N}_L(M^-, P^-)$ and $\mathcal{N}_L(\tilde{M}^m, P^m)$ respectively. It follows from the definition of $\mathcal{S}_{M_0}(w_0)$ that $\bar{\theta}^- = 0$.

Proof. According to Bayes' rule and the definition of CGDs,

the posterior attitude distribution is given by

$$p(R|\tilde{M}^m) \propto p(R)p(M^m = \tilde{M}^m|R) \\ \propto \exp \left\{ -\frac{1}{2} \left[\log((M^-)^T R)^\vee \right]^T (P^-)^{-1} \left[\log((M^-)^T R)^\vee \right] \right\} \times \\ \exp \left\{ -\frac{1}{2} \left[\log((\tilde{M}^m)^T R)^\vee \right]^T (P^m)^{-1} \left[\log((\tilde{M}^m)^T R)^\vee \right] \right\}$$

Letting $R(\theta) \in \mathcal{S}_{M^-}(w_0)$ and noting $M^-, \tilde{M}^m \in \mathcal{S}_{M^-}(w_0)$, we have

$$\log((M^-)^T R(\theta))^\vee = \theta w_0, \\ \log((\tilde{M}^m)^T R(\theta))^\vee = \log((\tilde{M}^m)^T (M^-)(M^-)^T R(\theta))^\vee \\ = w_0(\theta - \bar{\theta}^m).$$

The posterior distribution can then be rewritten as

$$p(R(\theta)|\tilde{M}^m) \\ \propto \exp \left\{ -\frac{1}{2} \theta w_0^T (P^-)^{-1} w_0 \theta \right\} \times \\ \exp \left\{ -\frac{1}{2} (\theta - \bar{\theta}^m) w_0^T (P^m)^{-1} w_0 (\theta - \bar{\theta}^m) \right\} \\ \propto \exp \left\{ -\frac{\theta^2}{2(\sigma^-)^2} \right\} \exp \left\{ -\frac{(\theta - \bar{\theta}^m)^2}{2(\sigma^m)^2} \right\} \propto C \exp \left\{ -\frac{(\theta - \bar{\theta}^+)^2}{2(\sigma^+)^2} \right\}$$

where $\bar{\theta}^+$ and σ^+ can be shown to be the same as (26a) and (26b). Therefore, the conclusion is verified. \square

The parameters $1/(\sigma^2)^+$ and θ^+ characterize the posterior distribution approximated by CGDs on $\mathcal{S}_{M_1}(w_0)$, and their expressions with respect to $1/(\sigma^-)^2$, θ^- , $1/(\sigma^m)^2$ and θ^m indicate the impact of the prior and the likelihood distributions on the posterior distribution.

C. Comparisons and discussions

The results given by Theorems III.3 and III.4 are summarized in Table I and the approximation introduced in Remark III.1 is used such that the parameters of both MFDs and CGDs are expressed with κ and $\bar{\theta}$. The trends of κ^+ as a function of $\Delta\bar{\theta} = \bar{\theta}^m - \bar{\theta}^-$, and $\bar{\theta}^+$ as a function of κ^m/κ^- with different $\Delta\bar{\theta}$ are shown in Figs. 2 and 3. Since the parameters are defined on $\mathcal{S}_{M^-}(w_0)$, we have $\bar{\theta}^- = 0$ and $\Delta\bar{\theta} = \bar{\theta}^m$.

TABLE I
MEAN ANGLES AND CONCENTRATION PARAMETERS OF DISTRIBUTIONS ON $\mathcal{S}_{M^-}(w_0)$

	MFDs	CGDs
κ^+	$\sqrt{(\kappa^-)^2 + (\kappa^m)^2 + 2\kappa^-\kappa^m \cos(\Delta\bar{\theta})}$	$\kappa^- + \kappa^m$
$\bar{\theta}^+$	$\text{sign}(\Delta\bar{\theta}) \arccos\left(\frac{\kappa^- + \kappa^+ \cos(\Delta\bar{\theta})}{\kappa^+}\right)$	$\frac{\kappa^m}{\kappa^- + \kappa^m} \Delta\bar{\theta}$

In this subsection, the parameters given by MFD-based Bayesian filters are denoted by κ_{MFD}^+ and $\bar{\theta}_{MFD}^+$, while the parameters given by CGD-based Bayesian filters are denoted by κ_{CGD}^+ and $\bar{\theta}_{CGD}^+$. Comparing κ_{MFD}^+ and κ_{CGD}^+ , it can

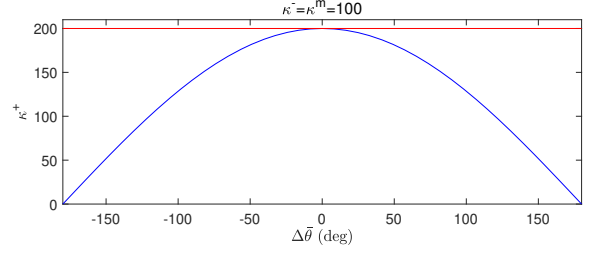


Fig. 2. The trend of κ^+ as a function of $\Delta\bar{\theta}$. Blue: κ^+ given by MFD-based Bayesian filters. Red: κ^+ given by CGD-based Bayesian filters

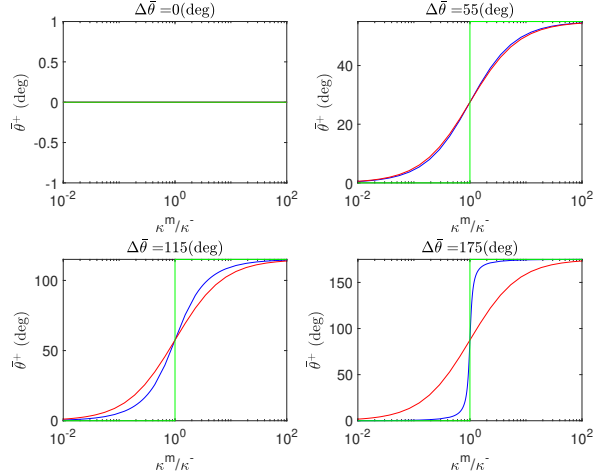


Fig. 3. The trends of $\bar{\theta}^+$ on κ^m/κ^- with different $\Delta\bar{\theta}$. Blue: $\bar{\theta}^+$ given by MFD-based Bayesian filters. Red: $\bar{\theta}^+$ given by CGD-based Bayesian filters. Green: the mean angle with higher confidence in $\bar{\theta}^-$ and $\bar{\theta}^m$

be seen from Table I and Fig. 2 that they are almost the same except for the term $\cos(\Delta\bar{\theta})$. Meanwhile, the closer $|\Delta\bar{\theta}|$ is to π , the closer κ_{MFD}^+ is to 0, i.e., the closer the posterior distribution on $\mathcal{S}_{M_1}(w_0)$ is to a uniform distribution. Therefore, the uncertainty in the posterior estimation provided by the Bayesian attitude filter with MFDs increases when there is a large discrepancy between the mean attitudes of the prior and the likelihood. In contrast, the uncertainty in the attitude filter with CGDs does not exhibit such an increase, since κ_{CGD}^+ is independent of $\Delta\bar{\theta}$. Besides, κ_{MFD}^+ and κ_{CGD}^+ are the same when $\Delta\bar{\theta} = 0$, which implies MFD-based and CGD-based filters give similar uncertainty descriptions around the axis w_0 when the mean attitude of the prior and the likelihood distributions are consistent.

Meanwhile, $\bar{\theta}_{MFD}^+$ and $\bar{\theta}_{CGD}^+$ are also different. Fig. 3 shows that $\bar{\theta}_{MFD}^+$ is always closer to the mean angles with a higher confidence, i.e., with larger concentration parameter, in $\bar{\theta}^-$ and $\bar{\theta}^m$. This difference is more significant when $\Delta\bar{\theta}$ is larger. The following presents an explanation from a theoretical perspective.

Proposition III.2. Define $\Delta\theta^+ \in \mathbb{R}$ as

$$\begin{aligned} \Delta\bar{\theta}^+(k, \Delta\bar{\theta}) &= \bar{\theta}_{MFD}^+ - \bar{\theta}_{CGD}^+ \\ &= \text{sign}(\Delta\bar{\theta}) \arccos\left(\frac{1 + k \cos \Delta\bar{\theta}}{\sqrt{1 + k^2 + 2k \cos(\Delta\bar{\theta})}}\right) - \frac{k}{1+k} \Delta\bar{\theta}, \end{aligned} \quad (27)$$

where $k = \kappa^m / \kappa^-$. Then the following property holds:

$$\Delta\bar{\theta}^+(k > 1, 0 < \Delta\bar{\theta} \leq \pi) > 0, \quad (28a)$$

$$\Delta\bar{\theta}^+(0 < k < 1, 0 < \Delta\bar{\theta} \leq \pi) < 0, \quad (28b)$$

$$\Delta\bar{\theta}^+(k > 1, -\pi \leq \Delta\bar{\theta} < 0) < 0, \quad (28c)$$

$$\Delta\bar{\theta}^+(0 < k < 1, -\pi \leq \Delta\bar{\theta} < 0) > 0, \quad (28d)$$

$$\lim_{k \rightarrow +\infty} \Delta\bar{\theta}^+ = \Delta\bar{\theta}^+(k = 0, 1) = 0. \quad (28e)$$

Proof. It is obvious that $\Delta\bar{\theta}^+(k, \Delta\bar{\theta} = 0) \equiv 0$ for any $k > 0$. Then, for $0 \leq \Delta\bar{\theta} \leq \pi$, the partial derivative of $\Delta\bar{\theta}^+(k, \Delta\bar{\theta})$ with respect to $\Delta\bar{\theta}$ is given by

$$\frac{\partial}{\partial \Delta\bar{\theta}} \Delta\bar{\theta}^+(k, \Delta\bar{\theta}) = \frac{k(k-1)(1 - \cos \Delta\bar{\theta})}{(1 + k^2 + 2k \cos \Delta\bar{\theta})(1+k)}.$$

Therefore, invoking $\Delta\bar{\theta}^+(k, \Delta\bar{\theta} = 0) \equiv 0$, we have

$$\begin{aligned} k < 1 &\Rightarrow \frac{\partial}{\partial \Delta\bar{\theta}} \Delta\bar{\theta}^+ < 0 \Rightarrow \Delta\bar{\theta}^+(k < 1, 0 \leq \theta \leq \pi) < 0, \\ k > 1 &\Rightarrow \frac{\partial}{\partial \Delta\bar{\theta}} \Delta\bar{\theta}^+ > 0 \Rightarrow \Delta\bar{\theta}^+(k > 1, 0 \leq \theta \leq \pi) > 0, \end{aligned}$$

verifying (28a) and (28b) respectively. Next, substituting $k = 1$ into $\Delta\bar{\theta}^+(k, \Delta\bar{\theta})$, we have

$$\begin{aligned} \Delta\bar{\theta}^+(k = 1) &= \text{sign}(\Delta\bar{\theta}) \arccos\left(\frac{1 + \cos \Delta\bar{\theta}}{\sqrt{2 + 2 \cos(\Delta\bar{\theta})}}\right) - \frac{1}{2} \Delta\bar{\theta} \\ &= \text{sign}(\Delta\bar{\theta}) \arccos\left(\frac{2 \cos^2(\Delta\bar{\theta}/2)}{\sqrt{4 \cos^2(\Delta\bar{\theta}/2)}}\right) - \frac{1}{2} \Delta\bar{\theta} = 0, \\ \Delta\bar{\theta}^+(k = 0) &= \text{sign}(\Delta\bar{\theta}) \arccos(1) - 0 = 0, \\ \lim_{k \rightarrow +\infty} \Delta\bar{\theta}^+ &= \text{sign}(\Delta\bar{\theta}) \arccos(\cos \Delta\bar{\theta}) - \Delta\bar{\theta} = 0, \end{aligned}$$

verifying (28e). Besides, because $\Delta\bar{\theta}^+(k, \Delta\bar{\theta})$ is an odd function with respect to $\Delta\bar{\theta}$, (28a) and (28b) can be easily extended to $\Delta\bar{\theta} \in [-\pi, \pi]$, which shows (28c) and (28d). Therefore, the conclusion is verified. \square

When $k > 1$, we have $\kappa^m > \kappa^-$, which means that measurements are more reliable than the prior information on $S_{M-}(w_0)$. According to (28), it is concluded that $\bar{\theta}_{MFD}^+$ is closer to $\bar{\theta}^m$ than $\bar{\theta}_{CGD}^+$. When $k < 1$, $\bar{\theta}_{MFD}^+$ is closer to $\bar{\theta}^-$ (i.e., 0) than $\bar{\theta}_{CGD}^+$. In a word, compared with the attitude filter with CGDs, the mean angle estimated by the Bayesian attitude filter with MFDs is always closer to the mean angle of a higher-confidence distribution (either the likelihood or the prior). Additionally, according to (28c), the mean angles given

by the two attitude filters are almost the same when κ^m and κ^- are the same or one is significantly larger than the other.

The differences in concentration parameters and mean angles both make the attitude filters with MFDs converge faster than those with CGDs, when initial errors are large. Since κ^+ depends on $\Delta\bar{\theta}$, the attitude filters with MFDs can detect the discrepancy between the predicted attitude and measurements, thereby quickly filtering out the negative effects of large initial errors by adjusting the uncertainty of attitude estimates. Meanwhile, according to Proposition III.2, MFD-based filters can filter out wrong information with low confidence faster, therefore leading to a faster convergence towards high confidence results than CGD-based filters.

The above conclusions are drawn from analytical solutions rather than limited numerical simulations or qualitative analysis and therefore possess certain generality. Meanwhile, these properties are derived merely from generic information fusion based on Bayes' rule with MFDs and CGDs, respectively. Therefore, the MFD-based filters propagating uncertainty with linearized equations and fusing information with Bayes' rule on $SO(3)$ can maintain the previously underlined advantages over the attitude filters with CGDs. This observation is leveraged in the next section to design novel fast nonlinear filters with MFDs.

D. Numerical examples

To illustrate the difference in Bayesian attitude filters with MFDs and CGDs more clearly, we present a numerical example. The initial prior distribution at $t = 0$ is set as $R_0 \sim \mathcal{M}(F_0)$ with $F_0 = 55 \exp((35\pi/36)w_0^\wedge)$ and $w_0 = [0.54, 0.54, 0.65]^T$, and the corresponding CGD is chosen as $R_0 \sim \mathcal{N}_{\mathcal{L}}(\exp((35\pi/36)w_0^\wedge), P_0)$ with $P_0 = 0.0091I_3$. The initial prior distribution is fused with the likelihood distribution twice via Bayes' rule at $t = 1$ and $t = 2$, and the posterior distribution at $t = 1$ is chosen as the prior distribution at $t = 2$. Since computing the full posterior distributions of Bayesian filters with CGDs is nontrivial, approximated posterior distributions are obtained with the first-order approximation of Baker-Campbell-Hausdorff formula, i.e. $\log(\exp(\xi^\wedge) \exp(\zeta^\wedge)) \approx \xi^\wedge + \zeta^\wedge$ for $\xi, \zeta \in \mathbb{R}^3$ and $\|\xi\|, \|\zeta\| \ll 1$. The likelihood distribution is set as $R_m | R_t \sim \mathcal{M}(R_t K_m)$ with $K_m = 60I_3$ for MFDs and $R_m | R_t \sim \mathcal{N}_{\mathcal{L}}(R_t, P_m)$ with $P_m = 0.0083I_3$ for CGDs. The true attitudes are set as $R_t = I_3$ for $t = 0, 1, 2$. These parameter settings imply that the attitude of a stationary rigid body, whose body-fixed frame coincides with the inertial frame, is estimated with a large initial error around the axis w_0 and direct attitude measurements. The measurements are independent of the initial error and therefore have higher confidence levels. The results are summarized in Table II and Fig. 4.

At $t = 0$, the prior and the likelihood distributions fed into the MFD-based and the CGD-based attitude filters are almost the same. However, after the first fusion at $t = 1$, the posterior distributions of the two filters are noticeably different, as shown in Figs. 4b and 4e. Their differences are twofold. Firstly, although the prior and the likelihood distributions are both highly concentrated about the mean

attitude, the posterior distribution given by the MFD-based attitude filter is significantly uncertain for rotations about the axis w_0 and κ also steeply decreases at $t = 1$. By contrast, the posterior distribution given by the CGD-based attitude filter is even more concentrated around the mean attitude than the prior and the likelihood distributions, as shown in Fig. 4f and Table II. As discussed in Section III-C, the reason for this difference is that the concentration parameter of the posterior CGD is independent of the mean angle, while that of MFDs is not. Secondly, the mean attitude of the MFD-based filter at $t = 1$ is closer to the mean attitude of the likelihood distribution than that of the CGD-based filter at $t = 1$, which corresponds to Proposition III.2. Then, at $t = 2$, the posterior distribution given by the MFD-based attitude filter is almost the same as the likelihood distribution because the prior distribution is highly uncertain for rotations about the axis w_0 , as shown in Fig. 4c. In contrast, as shown in Fig. 4f, the error of the CGD-based attitude filter is still large.

TABLE II

MEAN ANGLES AND CONCENTRATION PARAMETERS OF DISTRIBUTIONS ON $\mathcal{S}_{I_3}(w_0)$

Probabilistic Model		Likelihood	$t = 0$	$t = 1$	$t = 2$
MFDs	κ	120	110	14.16	123.71
	$\bar{\theta}$	0°	175°	42.62°	6.43°
CGDs	$1/\sigma^2$	120	110	230	350
	$\bar{\theta}$	0°	175°	83.70°	55°

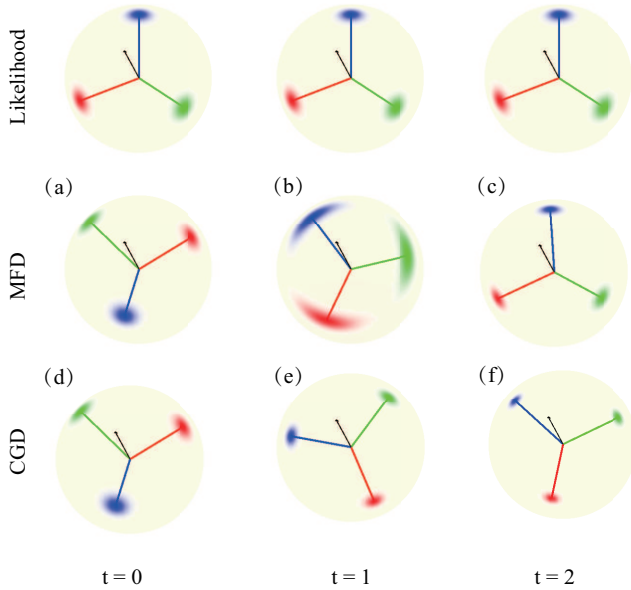


Fig. 4. The posterior distribution with several direct attitude measurements.

IV. MFD-BASED FAST NONLINEAR FILTERS FOR ATTITUDE ESTIMATION

In this section, we apply MFDs to characterize attitude error on $SO(3)$ and thereby propose two MFD-based fast nonlinear filters for attitude estimation.

A. Attitude estimation error following MFDs

We construct the following probability model to characterize the uncertainty of random attitudes with invariant attitude error following MFDs on $SO(3)$.

Definition IV.1. The discrepancy of the random matrix $R \in SO(3)$ with respect to $\bar{R} \in SO(3)$ is characterized by the left- or right-invariant error with MFDs on $SO(3)$ if it satisfies

$$R = \delta R \bar{R}, \quad \delta R \sim \mathcal{M}(N), \quad (29a)$$

or

$$R = \bar{R} \delta R, \quad \delta R \sim \mathcal{M}(N), \quad (29b)$$

where \bar{R} and $N = N^T \in \mathbb{R}^{3 \times 3}$ are deterministic parameters. For simplicity, (29a) and (29b) are denoted by $R \sim \mathcal{P}_{\mathcal{R}}\mathcal{M}(\bar{R}, N)$ and $R \sim \mathcal{P}_{\mathcal{L}}\mathcal{M}(\bar{R}, N)$, respectively.

The right-invariant error is invariant to right multiplications for any deterministic group element $\bar{R}_R \in SO(3)$, and the left-invariant error has similar invariance for left multiplications. The relationship between the above probability model and MFDs are presented as follows.

Proposition IV.1. Consider a random rotation matrix $R \sim \mathcal{M}(F)$ with $F \in \mathbb{R}^{3 \times 3}$ and the proper left and right decompositions of F are given by $F = K'M'$ and $F = MK$, respectively. Then, the probability model with invariant errors on $SO(3)$ is given respectively by

$$R \sim \mathcal{P}_{\mathcal{R}}\mathcal{M}(M', K') \text{ and } R \sim \mathcal{P}_{\mathcal{L}}\mathcal{M}(M, K).$$

Proof. For $R \sim \mathcal{P}_{\mathcal{R}}\mathcal{M}(M', K')$, we have

$$R = \delta R M', \quad \delta R \sim \mathcal{M}(K').$$

According to (8), we can obtain $R \sim \mathcal{M}(F')$, where $F' = K'M' = F$.

Similarly, for $R \sim \mathcal{P}_{\mathcal{L}}\mathcal{M}(M, K)$, we have

$$R = M \delta R, \quad \delta R \sim \mathcal{M}(K).$$

According to (8), we can obtain $R \sim \mathcal{M}(F'')$, where $F'' = MK = F$. \square

Let $\delta R = \exp(\xi^\wedge)$. When ξ is small, or equivalently the random error δR is highly concentrated about I_3 , we can establish a connection between N and the covariance of ξ .

Proposition IV.2. Let the rotation matrix δR be parameterized by the exponential map $\exp : \mathfrak{so}(3) \rightarrow SO(3)$ as $\delta R(\xi) = \exp(\xi^\wedge)$. Suppose that $\delta R \sim \mathcal{M}(N)$, and the proper SVD of N is given by $N = VSV^T$, where $S = \text{diag}[s_1, s_2, s_3]$. If $s_3 \gg 0$, then ξ follows a 3-dimensional Gaussian distribution with

$$\xi \sim \mathcal{N}(0, V(\text{tr}(S)I_3 - S)^{-1}V^T) \quad (30)$$

Proof. Let $\delta R' = V^T \delta R V$, $P = (\text{tr}(S)I_3 - S)^{-1} = \text{diag}[1/(s_2 + s_3), 1/(s_1 + s_3), 1/(s_1 + s_2)]$, and $\delta R' = \exp(\xi'^\wedge)$. Replacing δR with $\exp(\xi^\wedge)$, we can obtain

$$\exp(\xi'^\wedge) = \delta R' = V^T \exp(\xi^\wedge) V = \exp(V^T \xi^\wedge V),$$

which implies that $\xi' = V^T \xi$. According to (36) in [37], ξ' follows a Gaussian distribution with $\xi' \sim \mathcal{N}(0, P)$. Using $\xi' = V^T \xi$, we obtain $\xi \sim \mathcal{N}(0, V P V^T)$, which shows (30). \square

Correspondingly, N can be uniquely determined by the covariance matrix $P \in \mathbb{R}^{3 \times 3}$ of $\xi \sim \mathcal{N}(0, P)$ as

$$N = U \left(\frac{1}{2} \text{tr}(\Lambda^{-1}) I_3 - \Lambda^{-1} \right) U^T, \quad (31)$$

where U and Λ are given by the proper SVD of $P = U \Lambda U^T$.

The proposed probability model divides the random rotation matrix R into two mutually independent parts: a deterministic central attitude \bar{R} and a small random error δR . They can be separately handled. Additionally, the random error can be propagated and updated by a linearized error system and measurement equations. These characteristics will be utilized in the following attitude filter development.

B. Filtering with the right-invariant error on $SO(3)$

Consider the system with discrete attitude kinematics (13) and measurement model (14). The Bayesian filter with the right-invariant error approximates the posterior with (29a), i.e., we assume that the posterior probability of attitude at t_k is characterized by

$$R_k | \{\tilde{b}_k^i\} \sim \mathcal{P}_{\mathcal{RM}}(\hat{R}_k, N_k), \quad (32)$$

where \hat{R}_k and N_k are computed at each step as follows.

1) *Prior*: To obtain the prior attitude distribution, we analyze the deterministic central attitude and random right-invariant error along (13) separately.

Given \hat{R}_{k-1} , N_{k-1} and $\tilde{\omega}_k$, the central attitude at t_k , denoted by $\hat{R}_{k|k-1}$, is obtained from the deterministic part of (13), as

$$\hat{R}_{k|k-1} = \hat{R}_{k-1} \exp\{(h\tilde{\omega}_k)^\wedge\}. \quad (33)$$

Assuming that the prior probability of R_k is characterized by $R_k \sim \mathcal{P}_{\mathcal{RM}}(\hat{R}_{k|k-1}, N_{k|k-1})$, then we have

$$R_k = \delta R_{k|k-1} \hat{R}_{k|k-1}, \quad \delta R_{k|k-1} \sim \mathcal{M}(N_{k|k-1}), \quad (34)$$

Next, we compute $N_{k|k-1}$ with the linearized error equation. Assume that $\delta R_{k|k-1}$ is highly concentrated about I_3 and $\|w_k\|$ is small. Denoting by $\xi_{k|k-1} \in \mathbb{R}^3$, it follows that $\|\xi_{k|k-1}\| \ll 1$ and thus

$$\delta R_{k|k-1} = \exp(\xi_{k|k-1}^\wedge) = I + \xi_{k|k-1}^\wedge + \mathcal{O}(\|\xi_{k|k-1}\|^2). \quad (35)$$

Substituting (33) and (11) into (34), the estimation error is then derived as

$$\begin{aligned} \delta R_{k|k-1} &= R_{k-1} \exp\{(h\tilde{\omega}_k + w_k)^\wedge\} \exp\{(h\tilde{\omega}_k)^\wedge\}^T \hat{R}_{k-1}^T \\ &\approx \delta R_{k-1} \hat{R}_{k-1} \exp\{(w_k)^\wedge\} \hat{R}_{k-1}^T \\ &= \delta R_{k-1} \exp\{(\hat{R}_{k-1} w_k)^\wedge\} \end{aligned} \quad (36)$$

Employing (35) and retaining the first-order term, the linearization of (36) is computed as

$$\xi_{k|k-1} = \xi_{k-1} + \hat{R}_{k-1} w_k,$$

and the covariance matrix of $\xi_{k|k-1}$ is given by

$$P_{k|k-1} = P_{k-1} + \hat{R}_{k-1} Q_k \hat{R}_{k-1}^T, \quad (37)$$

where P_{k-1} is determined by the approximate relationship with $N_{k|k-1}$ in Proposition IV.2. Similarly, $N_{k|k-1}$ is computed with $P_{k|k-1}$ by (31) as

$$N_{k|k-1} = U_{k|k-1} \left(\frac{1}{2} \text{tr}(\Lambda_{k|k-1}^{-1}) I_3 - \Lambda_{k|k-1}^{-1} \right) U_{k|k-1}^T,$$

where $U_{k|k-1}$ and $\Lambda_{k|k-1}$ are given by the proper SVD of $P_{k|k-1} = U_{k|k-1} \Lambda_{k|k-1} U_{k|k-1}^T$.

2) *Likelihood*: The measurement update stage constructs a probability model defined by (29a) as the likelihood distribution, using measurement equations.

Consider the measurement model described by (14). For a given weight matrix $W_k = \text{diag}[w_k^1, \dots, w_k^n]$, the attitude measurement is generated by solving Wahba's problem with measurement vectors $\tilde{B}_k = [\tilde{b}_k^1, \dots, \tilde{b}_k^n]$ and reference vectors $E_k = [e_k^1, \dots, e_k^n]$, which is

$$\hat{R}_k^m(\tilde{B}_k, E_k) = \min_{\hat{R} \in SO(3)} \frac{1}{2} \text{tr}[(E_k - \hat{R}^T \tilde{B}_k)^T W_k (E_k - \hat{R}^T \tilde{B}_k)]. \quad (38)$$

One solution of Wahba's problem was given by [38], in which the proper SVD was used to compute the optimal attitude.

Lemma IV.1. [38] Define a matrix \tilde{L}_k as $\tilde{L}_k = E_k W_k \tilde{B}_k^T$. Then, the unique minimum to (38) is obtained as

$$\hat{R}_k^m = UV^T,$$

where U and V are given by the proper SVD $\tilde{L}_k = USV^T$. Furthermore, \hat{R}_k^m is unique when $s_2 + s_3 \neq 0$.

We assume that the optimal attitude is always unique and its uncertainty is characterized by the conditional probability distribution

$$\hat{R}_k^m | R_k \sim \mathcal{P}_{\mathcal{RM}}(R_k, N_k^m), \quad (39)$$

where N_k^m is the parameter to be computed. The actual attitude R_k and vectors B_k in \mathcal{F}_B corresponding to E_k can be rewritten into

$$R_k = \delta R_k^T \hat{R}_k^m, \quad \delta R_k \sim \mathcal{M}(N_k^m), \quad (40)$$

$$B_k = \tilde{B}_k + \delta B_k, \quad \delta B_k = [\delta b_k^1, \dots, \delta b_k^n]. \quad (41)$$

According to [?], the optimal attitude \hat{R}_k^m satisfies

$$\tilde{L}_k^T \hat{R}_k^m = (\hat{R}_k^m)^T \tilde{L}_k, \quad (42)$$

and $L_k = E_k W_k B_k^T$ satisfies

$$L_k^T R_k = R_k^T L_k. \quad (43)$$

Equation (43) is linearized with $\xi_k^m = \log(\hat{R}_k^m R_k^T)^\vee$ to compute N_k^m as summarized in the following theorem.

Theorem IV.1. Consider a unique $\hat{R} \in SO(3)$ satisfying (42) with measurement vectors $\tilde{B} = [\tilde{b}^1, \dots, \tilde{b}^n]$, reference vectors $E = [e^1, \dots, e^n]$ and a weight matrix $W = \text{diag}[w^1, \dots, w^n]$. The actual attitude and vectors in \mathcal{F}_B corresponding to E are defined as (40) and (41) respectively. The first-order approximation of (43) with errors $\xi = \log(\hat{R} R^T)^\vee \in \mathbb{R}^3$ and $\delta B = [\delta b^1, \dots, \delta b^n]$ is

$$\left(\text{tr}(\tilde{L} \hat{R}^T) I_3 - \tilde{L} \hat{R}^T \right) \xi = \sum_i w^i (e^i)^\wedge \hat{R} \delta b^i, \quad (44)$$

where $\tilde{L} = EW\tilde{B}^T$.

Proof. Substituting (40), (41) and (35) into (43) and retaining the first-order term, we have

$$\hat{R}^T \xi^\wedge \tilde{L} + \tilde{L}^T \xi^\wedge \hat{R} = \delta B W E^T \hat{R} - \hat{R}^T E W \delta B^T. \quad (45)$$

Multiplying \hat{R} and \hat{R}^T to the left and right sides of (45) yields

$$\xi^\wedge \tilde{L} \hat{R}^T + \hat{R} \tilde{L}^T \xi^\wedge = \hat{R} \delta B W E^T - E W (\hat{R} \delta B)^T. \quad (46)$$

Applying (2) to the left side of (46), expanding the right of (46) and applying (3), we have

$$\begin{aligned} & \left[\text{tr} \left(\tilde{L} \hat{R}^T \right) I_3 - \tilde{L} \hat{R}^T \right] \xi \\ &= \sum_i^n w^i \left[\left(\hat{R} \delta b^i \right) (e^i)^T - e^i \left(\hat{R} \delta b^i \right)^T \right] = \sum_i^n w_i (e^i)^\wedge \hat{R} \delta b^i, \end{aligned}$$

which gives (44). \square

Theorem IV.1 establishes a linear map between ξ and δb_i , and it is a bijection when the optimal attitude given by (38) is unique.

Proposition IV.3. Suppose that the optimal attitude given by (38) is unique, or equivalently, $s_2 + s_3 \neq 0$. Denoting by $A = \text{tr} \left(\tilde{L} \hat{R}^T \right) I_3 - \tilde{L} \hat{R}^T$ in (44), then A is invertible.

Proof. Because $s_1 \geq s_2 \geq |s_3|$ and $s_2 + s_3 \neq 0$, it follows $s_1 + s_2 \geq s_1 + s_3 \geq s_2 + s_3 > 0$. Furthermore, we have

$$\begin{aligned} \det(A) &= \det \left(\text{tr} \left(\tilde{L} \hat{R}^T \right) I_3 - \tilde{L} \hat{R}^T \right) \\ &= \det \left(\text{tr} \left(U S V^T V U^T \right) U I_3 U^T - U S V^T V U^T \right) \\ &= \det \left(U \text{diag}[s_2 + s_3, s_1 + s_3, s_1 + s_2] U^T \right) \\ &= (s_2 + s_3)(s_1 + s_3)(s_1 + s_2) > 0. \end{aligned}$$

Therefore, the matrix A is invertible. \square

Proposition IV.3 implies that A_k is invertible and thus equation (44) can be rewritten into

$$\xi_k^m = \sum_i^n w^i A_k^{-1} (e_k^i)^\wedge \hat{R}_k^m \delta b_k^i,$$

and the covariance matrix of ξ_k^m is given by

$$P_k^m = \sum_i^n (w^i)^2 \left(A_k^{-1} (e_k^i)^\wedge \hat{R}_k^m \right) G_k^i \left(A_k^{-1} (e_k^i)^\wedge \hat{R}_k^m \right)^T.$$

Then N_k^m can be computed with P_k^m by (31).

3) Posterior: The posterior probability of the attitude is constructed by Bayes' rule with the prior and the likelihood as follows.

Theorem IV.2. Suppose that the a priori attitude distribution of R is given by $\mathcal{P}_{\mathcal{R}}\mathcal{M}(R^-, N^-)$ with a mean attitude $R^- \in SO(3)$ and $N^- = (N^-)^T \in \mathbb{R}^{3 \times 3}$. Consider an attitude measurement R^m satisfying $R^m | R \sim \mathcal{P}_{\mathcal{R}}\mathcal{M}(R, N^m)$ with $R \in SO(3)$ and $N^m = (N^m)^T \in \mathbb{R}^{3 \times 3}$. Then, the posterior attitude distribution with a measurement $R^m = \tilde{R}^m$ is characterized by,

$$R | \tilde{R}^m \sim \mathcal{P}_{\mathcal{R}}\mathcal{M}(R^+, N^+), \quad (47)$$

where R^+ and N^+ are the polar and the elliptical components from the proper left polar decomposition of $F = N^- R^- + N^m \tilde{R}^m$ respectively.

Proof. Substituting $p(R)$ and $p(\tilde{R}^m | R)$ into Bayes' rule

$$p \left(R | \tilde{R}^m \right) \propto p(R) p(\tilde{R}^m | R),$$

we can obtain

$$\begin{aligned} p \left(R | \tilde{R}^m \right) &\propto \text{etr} \left[\left(N^- R^- \right)^T R + \left(N^m \tilde{R}^m \right)^T \tilde{R}^m \right] \\ &= \text{etr} \left[\left(N^- R^- + N^m \tilde{R}^m \right)^T R \right], \end{aligned}$$

which implies that $R | \tilde{R}^m \sim \mathcal{M}(N^- R^- + N^m \tilde{R}^m)$. Let $F = N^- R^- + N^m \tilde{R}^m$ and denote the proper left polar decomposition of F by $F = N^+ R^+$. According to (29a), we have $R | \tilde{R}^m \sim \mathcal{P}_{\mathcal{R}}\mathcal{M}(R^+, N^+)$, which gives (47). \square

Because the updating frequency of vector measurements is often lower than that of gyros in practice, the propagation step will be executed in a loop until new measurement vectors are available. The pseudo-code for the proposed estimation scheme is presented in Algorithm 1.

Algorithm 1 Filtering with the right-invariant error

```

1: procedure ESTIMATION  $\hat{R}_k$ 
2:   Let  $k = 0, R_0 \sim \mathcal{P}_{\mathcal{L}}\mathcal{M}(\hat{R}_0, N_0)$ 
3:   loop
4:      $k = k + 1$ 
5:      $\hat{R}_{k|k-1} = \hat{R}_{k-1} \exp\{(\tilde{h}\tilde{\omega}_k)^\wedge\}$ 
6:     Compute  $P_{k-1}$  with  $N_{k-1}$  in Proposition IV.2 and
        $P_{k|k-1}$  with  $P_{k-1}$  and  $Q_k$  from (37)
7:     Compute the proper SVD of  $P_{k|k-1}$  as  $P_{k|k-1} =$ 
        $U_{k|k-1} \Lambda_{k|k-1} U_{k|k-1}^T$ 
8:      $N_{k|k-1} = U_{k|k-1} \left( \frac{1}{2} \text{tr}(\Lambda_{k|k-1}^{-1}) I_3 - \Lambda_{k|k-1}^{-1} \right) U_{k|k-1}^T$ 
9:     if  $\tilde{B}_k$  is available then
10:       $\tilde{L}_k = E_k W_k \tilde{B}_k^T$ 
11:      Compute the proper left polar decomposition
       of  $\tilde{L}_k$  as  $\tilde{L}_k = K_k^m M_k^m$  and  $\hat{R}_k^m = U_k^m (V_k^m)^T$ 
12:       $P_k^m = \sum_i^n (w^i)^2 \left( A^{-1} (e^i)^\wedge \hat{R} \right) G_k^i \left( A^{-1} (e^i)^\wedge \hat{R} \right)^T$ 
13:      Compute the proper SVD of  $P_k^m$  as  $P_k^m =$ 
        $U_k^m \Lambda_k^m (U_k^m)^T$ 
14:       $N_k^m = U_k^m \left( \frac{1}{2} \text{tr}((\Lambda_k^m)^{-1}) I_3 - (\Lambda_k^m)^{-1} \right) (U_k^m)^T$ 
15:       $F_k = N_k^m \hat{R}_k^m + N_{k|k-1} \hat{R}_{k|k-1}$ 
16:      Compute  $N_k$  and  $\hat{R}_k$  by the proper left polar
       decomposition of  $F_k$  as  $F_k = N_k \hat{R}_k$ 
17:    else
18:       $\hat{R}_k = \hat{R}_{k|k-1}, N_k = N_{k|k-1}$ 
19:    end if
20:  end loop
21: end procedure

```

C. Filtering with the left-invariant error on $SO(3)$

The preceding attitude filter with the left-invariant error is designed based on the uncertainty model defined by (29b).

Similarly, we can also derive a filter by approximating the underlying posterior distribution of attitudes with (29b), i.e.,

$$R_k|\{\tilde{b}_k^i\} \sim \mathcal{P}_{\mathcal{LM}}(\hat{R}_k, N_k), \quad \delta R = \hat{R}^T R. \quad (48)$$

1) Prior: For given \hat{R}_{k-1} and $\tilde{\omega}_k$, the central attitude $\hat{R}_{k|k-1}$ is obtained by the deterministic part of the kinematics, or equivalently, by (33).

Next, $N_{k|k-1}$ is derived from linearized error equations with redefined δR in (48) as follows. Substituting (33) and (11) into (48), we have

$$\begin{aligned} \delta R_{k|k-1} &= \exp\{(h\tilde{\omega}_k)^\wedge\}^T \hat{R}_{k-1}^T R_{k-1} \exp\{(h\tilde{\omega}_k + w_k)^\wedge\} \\ &= \exp\{(h\tilde{\omega}_k)^\wedge\}^T \delta R_{k-1} \exp\{(h\tilde{\omega}_k + w_k)^\wedge\} \end{aligned}$$

Assuming the time step h and error δR to be small, employing (35) and retaining the first-order term, the linearized error equation is derived as

$$\xi_{k|k-1} = \exp\{(h\tilde{\omega}_k)^\wedge\}^T \xi_{k-1} + w_{k-1},$$

and the covariance matrix of $\xi_{k|k-1}$ is given by

$$P_{k|k-1} = \exp\{(h\tilde{\omega}_k)^\wedge\}^T P_{k-1} \exp\{(h\tilde{\omega}_k)^\wedge\} + Q_k. \quad (49)$$

which, together with (31), can be used to compute $P_{k|k-1}$.

2) Likelihood: For measurement updates, the attitude measurement is obtained uniquely from solving Wahba's problem using SVD method with \tilde{B}_k and E_k , and follows

$$\hat{R}_k^m | R_k \sim \mathcal{P}_{\mathcal{LM}}(R_k, N_k^m), \quad (50)$$

where N_k^m is computed using (42) and the linearized system equation with the left-invariant error $\delta R_k = \hat{R}_k^m R_k^T$ as follows.

Theorem IV.3. Consider a unique $\hat{R} \in SO(3)$ satisfying (42) with measurement vectors $\tilde{B} = [\tilde{b}^1, \dots, \tilde{b}^n]$, reference vectors $E = [e^1, \dots, e^n]$ and a weight matrix $W = \text{diag}[w^1, \dots, w^n]$. The first-order approximation of (43) with $\delta R = \hat{R} R^T$ and $\delta B = [\delta b^1, \dots, \delta b^n]$ satisfying (41) is

$$\left(\text{tr}(\hat{R}^T \tilde{L}) I_3 - \hat{R}^T \tilde{L} \right) \xi = \sum_i w^i (\hat{R}^T e^i)^\wedge \delta b^i, \quad (51)$$

where $\xi = \log(\delta R)^\vee \in \mathbb{R}^3$ and $\tilde{L} = EW\tilde{B}^T$.

Proof. Substituting (40), $\delta R_k = \hat{R}_k^m R_k^T$ and (35) into (43) and retaining the first-order term, we have

$$\xi^\wedge \hat{R}^T \tilde{L} + \tilde{L}^T \hat{R} \xi^\wedge = \delta B W E^T \hat{R} - \hat{R}^T E W \delta B^T. \quad (52)$$

Applying (2) to the left side of (52), expanding the right side of the (52) and applying (3), we have

$$\begin{aligned} \left[\text{tr}(\hat{R}^T \tilde{L}) I_3 - \hat{R}^T \tilde{L} \right] \xi &= \sum_i^n w^i \left[\delta b^i (\hat{R}^T e^i)^T - \hat{R}^T e^i (\delta b^i)^T \right] \\ &= \sum_i^n w^i (\hat{R}^T e^i)^\wedge \delta b_i, \end{aligned}$$

which gives (51). \square

Next, we prove the invertibility of the matrix $\text{tr}(\hat{R}^T \tilde{L}) I_3 - \hat{R}^T \tilde{L}$ such that a linear bijection can be established.

Proposition IV.4. Suppose that the optimal attitude given by (38) is unique, or equivalently, $s_2 + s_3 \neq 0$. Denoting $B = \text{tr}(\hat{R}^T \tilde{L}) I_3 - \hat{R}^T \tilde{L}$ in (51), then B is invertible.

Proof. Because $s_1 \geq s_2 \geq |s_3|$ and $s_2 + s_3 \neq 0$, $s_1 + s_2 \geq s_1 + s_3 \geq s_2 + s_3 > 0$. Furthermore, we have

$$\begin{aligned} \det(B) &= \det\left(\text{tr}(\hat{R}^T \tilde{L}) I_3 - \hat{R}^T \tilde{L}\right) \\ &= \det(V \text{tr}[s_2 + s_3, s_1 + s_3, s_1 + s_2] V^T) \\ &= (s_2 + s_3)(s_1 + s_3)(s_1 + s_2) > 0. \end{aligned}$$

Therefore, the matrix B is invertible. \square

Using (51), the covariance matrix of ξ_k^m is given by

$$P_k^m = \sum_i^n (w^i)^2 \left(A_k^{-1} \left((\hat{R}_k^m)^T e_k^i \right)^\wedge \right) G_k^i \left(A_k^{-1} \left((\hat{R}_k^m)^T e_k^i \right)^\wedge \right)^T.$$

3) Posterior: Similarly to the proposed filter with the right-invariant error, the following theorem is presented to compute the parameters of the posterior distribution.

Theorem IV.4. Suppose that the a priori attitude distribution of R is given by $\mathcal{P}_{\mathcal{LM}}(R^-, N^-)$ with a central attitude $R^- \in SO(3)$ and $N^- \in \mathbb{R}^{3 \times 3}$. Consider an attitude measurement R^m satisfying $R^m | R \sim \mathcal{P}_{\mathcal{RM}}(R, N^m)$ with $N^m = (N^m)^T \in \mathbb{R}^{3 \times 3}$. Then, the posterior attitude distribution with a measurement $R^m = \tilde{R}^m$ is characterized by

$$R | \tilde{R}^m \sim \mathcal{P}_{\mathcal{LM}}(R^+, N^+), \quad (53)$$

where R^+ and N^+ are the polar and the elliptical components from the proper right polar decomposition of $F = R^- N^- + \tilde{R}^m N^m$ respectively.

Proof. Substituting $p(R)$ and $p(\tilde{R}^m | R)$ into Bayes' rule and similarly to the proof of Theorem IV.2, we can obtain

$$\begin{aligned} p(R | \tilde{R}^m) &\propto \text{etr} \left[(R^- N^-)^T R + (R N^m)^T \tilde{R}^m \right] \\ &= \text{etr} \left[\left(R^- N^- + \tilde{R}^m N^m \right)^T R \right], \end{aligned}$$

which implies that $R | \tilde{R}^m \sim \mathcal{M}(R^- N^- + \tilde{R}^m N^m)$. Let $F = R^- N^- + \tilde{R}^m N^m$ and denote the right polar decomposition of F by $F = R^+ N^+$. According to (29b), we have $R | R^m \sim \mathcal{P}_{\mathcal{RM}}(R^+, N^+)$, which gives (53). \square

The pseudo code for the filter with the left-invariant error is summarized in Algorithm 2.

D. Discussions

The two proposed estimation methods are partially similar to the IEKF in [21] and the Bayesian estimator in [33] but differ greatly in some critical steps. More precisely, our methods utilize linearized error equations and two newly defined probability models to approximate the underlying prior and likelihood distributions on $SO(3)$. As a result, they are closed-form and avoid solving nonlinear equations to

Algorithm 2 Filter with the left-invariant error

```

1: procedure ESTIMATION  $\hat{R}_k$ 
2:   Let  $k = 0, R_0 \sim \mathcal{P}_{\mathcal{L}}\mathcal{M}(\hat{R}_0, N_0)$ 
3:   loop
4:      $k = k + 1$ 
5:      $\hat{R}_{k|k-1} = \hat{R}_{k-1} \exp\{(h\tilde{\omega}_k)^\wedge\}$ 
6:     Compute  $P_{k-1}$  with  $N_{k-1}$  in Proposition IV.2 and
        $P_{k|k-1}$  with  $P_{k-1}$  and  $Q_k$  from (49)
7:     Compute the proper SVD of  $P_{k|k-1}$  as  $P_{k|k-1} =$ 
        $U_{k|k-1} \Lambda_{k|k-1} U_{k|k-1}^T$ 
8:      $N_{k|k-1} = V_{k|k-1} \left( \frac{1}{2} \text{tr}(\Lambda_{k|k-1}^{-1}) I_3 - \Lambda_{k|k-1}^{-1} \right) V_{k|k-1}^T$ 
9:     if  $\tilde{B}_k$  is available then
10:       $\tilde{L}_k = E_k W_k \tilde{B}_k^T$ 
11:      Compute the proper left polar decomposition
       of  $\tilde{L}_k$  as  $\tilde{L}_k = K_k^m M_k^m$  and  $\hat{R}_k^m = U_k^m (V_k^m)^T$ 
12:       $P_k^m = \sum_i^n w_i^2 \left( A^{-1}(e^i)^\wedge \hat{R} \right) G_k^i \left( A^{-1}(e^i)^\wedge \hat{R} \right)^T$ 
13:      Compute the proper SVD of  $P_k^m$  as  $P_k^m =$ 
        $V_k^m \Lambda_k^m (V_k^m)^T$ 
14:       $N_k^m = V_k^m \left( \frac{1}{2} \text{tr}((\Lambda_k^m)^{-1}) I_3 - (\Lambda_k^m)^{-1} \right) (V_k^m)^T$ 
15:       $F_k = \hat{R}_k^m N_k^m + \hat{R}_{k|k-1} N_{k|k-1}$ 
16:      Compute  $N_k$  and  $\hat{R}_k$  by the proper right polar
       decomposition of  $F_k$  as  $F_k = \hat{R}_k N_k$ 
17:    else
18:       $\hat{R}_k = \hat{R}_{k|k-1}, N_k = N_{k|k-1}$ 
19:    end if
20:  end loop
21: end procedure

```

obtain parameters from the first moment, significantly reducing computational complexity compared to the MFD-based filter in [33] that requires moment matching or unscented transformation.

The computational complexity of the proposed filter in Algorithm 1 is contributed by the proper SVD, matrix exponential function, addition, and multiplication. Since the proper SVD for 3×3 symmetric matrix and the matrix exponential function for 3×3 anti-symmetric matrix admit closed-form solutions, their computational costs are constant, i.e. $O(1)$. Therefore, the overall per-step complexity is mainly dominated by the computation of \tilde{L}_k , which scales linearly as $O(n)$, where n is the number of reference vectors. For the first-order estimator, however, additional complexity is caused by solving

$$\frac{1}{c(S)} \frac{\partial c(S)}{\partial s_i} - d_i = 0, \text{ for } i = \{1, 2, 3\}, \quad (54)$$

with the Newton-Armijo iteration, as present in [41], in moment matching. Each iteration needs to compute $c(S)$, $\partial c(S)/\partial s_i$, $\partial^2 c(S)/\partial^2 s_i s_j$ by the integration of modified Bessel functions, whose complexity scales linearly with the number of quadrature points, denoted by n_q . If the average number of trials to satisfy the Armijo line search is denoted by n_L , and assuming that the solver converges within n_I iterations, the per-step computational complexity of the first-order estimator is $O(n_I(1 + n_L)n_q) + O(n_z)$, where the term "1" represents the cost of computing the descent direction.

Thus, the extra computational cost of the first-order estimator is $O(n_I(1 + n_L)n_q)$. It is notable that there is *no* theory guarantees that the Newton-Armijo iteration terminates in a finite number of steps and n_I , as a result, can be very large. Even if n_I is bounded by a n_I^{max} , such as $n_I^{max} = 100$ in [41], $O(n_I(1 + n_L)n_q)$ is still larger than $O(n_z)$ because n_q is usually set to $50 \sim 100$ to promise accuracy, but n_z can be a single digit.

Moreover, while the linearized error equations evolve on \mathbb{R}^3 , the propagated central attitude and covariance matrix are used to compute the parameters of the two MFD-based probability models given by (29a) and (29b) on $SO(3)$, which approximate the underlying prior and likelihood distributions, respectively. As shown in Section III-C, the two key properties inducing the advantages of MFD-based attitude filters rely merely on the information fusion based on Bayes' rule with MFDs. These properties guarantee the theoretical stability of the proposed filters, as discussed in the next section.

It should be acknowledged that linearization, while improving computational speed, results in a theoretical loss of accuracy. For the estimator in [33], $O(h^{1.5})$ is omitted in moment propagation. In error equations (36) and (44), instead, high order terms $O(\|\xi\|^2)$ and $O(h^2)$ are omitted. Since ξ represents estimation error, $O(\|\xi\|^2)$ can be non-negligible when the uncertainty is large, even if h is small. However, this does not imply that the estimator in [33] is always more accurate than the proposed filter. The numerical solution of (??) cannot guarantee convergence within the specified n_I^{max} , leading to accuracy loss that cannot be precisely computed. In the measurement update, the proposed filter omitting $O(\|\xi\|^2)$ is to handle non-unit vector measurements and anisotropic Gaussian measurement noise, which are not considered by the estimator in [33] and can also lead to accuracy differences. Moreover, leveraging the closed-form iteration and the two key properties discussed in Section III-C, the filter guarantees the theoretical stability of the proposed filters, as discussed in the next section, while the estimator in [33] cannot. The two estimators with MFDs are further compared with simulations in Section VI.

V. THE PROPOSED FILTER AS A STABLE OBSERVER

Benefiting from the closed-form iterations and invariant error, the proposed filter with right-invariant error guarantees almost-global exponential stability under specific circumstances, which *no* existing filters with directional statistics achieve. This section provides the stability properties of the proposed filter as a deterministic observer for single-axis rotational motion of a rigid body.

A. The filter for single-axis rotation system

Without loss of generality, we consider a rigid body rotating about b_3 with an initial attitude $R_0 = \exp(\theta_0 b_3^\wedge)$, i.e., $R_k \in \mathcal{S}_{I_3}(b_3)$. Other single-axis rotational motions can be transferred to be about b_3 through coordinate transformation. The filter estimates attitudes using noise-free angular velocity measurements as well as direct attitude measurements, and

vector measurements can be reconstructed to attitude measurements by Lemma IV.1 and Theorem IV.1. Then, the filter can be rewritten in one-dimensional form on $S_{I_3}(b_3)$ using the following theorem.

Theorem V.1. *Given initial parameters $\hat{R}_0 = \exp(\hat{\theta}_0 b_3^\wedge)$, $N_0 = \text{diag}[\kappa_0, \kappa_0, \kappa_0^*]$ for $\kappa_0, \kappa_0^* > 0$, and measurement parameters $Q_k = \text{diag}[\sigma_k^*, \sigma_k^*, \sigma_k]$, $N_k^m = \text{diag}[\kappa_k^m, \kappa_k^m, \kappa_k^{m*}]$ for $\sigma_k, \sigma_k^*, \kappa_k^m, \kappa_k^{m*} > 0$, the filter in Algorithm 1 with angular velocity measurement $\tilde{\omega}_k = \tilde{\omega}_k b_3$ and attitude measurement $R_k^m = R_0 \exp(\theta_k^m b_3^\wedge)$ can be rewritten as*

$$\hat{R}_{k|k-1} = \exp(\hat{\theta}_{k|k-1} b_3^\wedge), \quad (55)$$

$$N_{k|k-1} = \text{diag}[\kappa_{k|k-1}, \kappa_{k|k-1}, \kappa_{k|k-1}^*], \quad (56)$$

$$\hat{R}_k = \exp(\hat{\theta}_k b_3^\wedge), \quad N_k = \text{diag}[\kappa_k, \kappa_k, \kappa_k^*], \quad (57)$$

where

$$\hat{\theta}_{k|k-1} = \hat{\theta}_{k-1} + \tilde{\omega}_k h, \quad \kappa_{k|k-1} = \frac{\kappa_{k-1}}{1 + 2\kappa_{k-1}\sigma_k}, \quad (58)$$

$$\kappa_k = \sqrt{(\kappa_{k|k-1})^2 + (\kappa_k^m)^2 + 2\kappa_{k|k-1}\kappa_k^m \cos(\theta_k^m - \hat{\theta}_{k|k-1})}, \quad (59)$$

$$\hat{\theta}_k = \hat{\theta}_{k|k-1} +$$

$$\text{sign}(\theta_k^m - \hat{\theta}_{k|k-1}) \arccos \left[(\kappa_{k|k-1} + \kappa_k^m \cos(\theta_k^m - \hat{\theta}_{k|k-1})) / \kappa_k \right], \quad (60)$$

and

$$\kappa_{k|k-1}^* = \frac{\kappa_{k-1|k-1} + \kappa_{k-1|k-1}^*}{1 + \sigma_k^* (\kappa_{k-1|k-1} + \kappa_{k-1|k-1}^*)} - \frac{\kappa_{k-1|k-1}}{1 + 2\kappa_{k-1|k-1}\sigma_k}, \quad (61)$$

$$\kappa_{k|k}^* = \kappa_{k|k-1}^* + \kappa_k^{m*}. \quad (62)$$

Proof. See Appendix A. \square

For single-axis rotational motion, Theorem V.1 provides a one-dimensional parameter representation of the filter with $\kappa_{k|k-1}, \hat{\theta}_{k|k-1}, \kappa_k, \hat{\theta}_k$ on $S_{I_3}(b_3)$, and indicates that the attitude estimates are independent of $\kappa_{k|k-1}^*, \kappa_k^*, \kappa_k^{m*}$ and σ_k^* . Moreover, the posterior parameters κ_k and $\hat{\theta}_k$ are the same as the posterior mean angle $\hat{\theta}^+$ and concentration parameter κ^+ , implying that the nonlinear filtering mechanism discussed in Section III is faithfully reflected in the filter for single-axis rotation. Next, we focus on the one-dimensional filter on $S_I(b_3)$ and show how the filtering mechanism guarantees almost-global exponential stability.

B. Stability analysis

Using the Frobenius norm, the attitude estimation error is defined as $\|R_k - \hat{R}_k\|_F = 2\text{tr}(I - R_k \hat{R}_k^T)$. For single-axis rotation, the error can be rewritten as $\|R_k - \hat{R}_k\|_F = 2[1 - \cos(\theta_k - \hat{\theta}_k)] \in [0, 4]$.

Combining the concentration parameter and estimation error, define a candidate Lyapunov function by

$$V_k = \kappa_k [1 - \cos(\theta_k - \hat{\theta}_k)]. \quad (63)$$

The following theorem proves that V_k is bounded by two positive definite functions and has exponential decay for all $\|R_k - \hat{R}_k\|_F < 4$ and $k \geq 0$.

Theorem V.2. *Consider the single-axis rotation $R_k = \exp(\theta_k b_3^\wedge)$ with noise-free measurement $R_k^m = \exp(\theta_k^m b_3^\wedge)$. If there exists $\alpha_1, \alpha_2, \beta_1, \beta_2 > 0$ such that $\alpha_1 < \sigma_k < \alpha_2$, $\beta_1 < \kappa_k < \beta_2$, $\forall k \geq 0$, then the one-dimensional filter in Theorem V.1 is almost-global exponential stability. More specifically, $\forall \hat{R}_0 \in S_I(b_3)$ such that $\|R_0 - \hat{R}_0\|_F \leq 4 - \epsilon$ for $\epsilon \in [0, 4)$, there is*

$$\|R_k - \hat{R}_k\|_F \leq C f(\epsilon)^k \|R_0 - \hat{R}_0\|_F, \quad (64)$$

where C is a constant and $f(\epsilon) < 1$ is a function with respect to ϵ and independent of k .

Proof. See Appendix B. We present a brief proof outline here. We first establish the monotonicity of V_k as $V_k \leq V_{k|k-1} = V_{k-1}/(1 + 2\kappa_{k-1}\sigma_k)$. Then, the boundedness of V_k is considered. The estimation error is proved to monotonically decrease as k increases as

$$1 - \cos(\theta_k - \hat{\theta}_k) < 1 - \cos(\theta_k - \hat{\theta}_{k|k-1}) = 1 - \cos(\theta_{k-1} - \hat{\theta}_{k-1}). \quad (65)$$

Using the monotonicity and viewing κ_k as a function with respect to $\kappa_{k|k-1}$, κ_k^m and $\cos(\theta_k - \hat{\theta}_{k|k-1})$, V_k is bounded by $\gamma_1 (1 - \cos(\theta_k - \hat{\theta}_k)) \leq V_k \leq \gamma_2 (1 - \cos(\theta_k - \hat{\theta}_k))$, where γ_1 and γ_2 are composed of $\alpha_1, \alpha_2, \beta_1, \beta_2$ and ϵ , and independent of k . Finally, combining the monotonicity and boundedness of V_k , (64) is verified as

$$\|R_k - \hat{R}_k\|_F \leq \frac{\kappa_0}{\gamma_2 \left(1 + 2\alpha_2\beta_1\sqrt{\epsilon - \frac{\epsilon^2}{4}}\right)^k} \|R_0 - \hat{R}_0\|_F. \quad (66)$$

Theorem V.2 provides a theoretical guarantee for the rapid convergence of the proposed filter under large initial error and gives an upper bound on the convergence speed, benefiting from its closed-form iteration and nonlinear filtering mechanism. None of the existing estimators with directional statistics provide theoretical stability because they rely on the numerical solution, which lacks proven finite-step convergence.

VI. NUMERICAL SIMULATIONS

This section compares the proposed fast nonlinear filters, the MFD-based filters in [33] and [37], and the IEKF [21]. For simplicity, we abbreviate our fast nonlinear filters with MFDs derived from the right- and left-invariant error by FNF-R and FNF-L, the Bayesian filter with MFDs in [33] by BF-MFD, the Bayesian filter with approximated MFDs by BF-AMFD [37]. Similarly to [33], a 3D pendulum is adopted to generate true attitude and angular velocity for numerical simulations. The initial attitude and angular velocity are given as $R_0 = I_{3 \times 3}$ and $\Omega_0 = 4.14 \times [1, 1, 1]^T \text{ rad/s}$ respectively. The attitude is assumed to be estimated with angular velocity and vector measurements at 50 Hz and 10 Hz respectively. The white noise of angular velocity measurements is Gaussian

TABLE III
AE (\pm SD) AND TIME CONSUMPTION: SMALL INITIAL ERRORS

Measurement Model		FNF-R	FNF-L	BF-MFD	BF-AMFD	IEKF	Mea
(i)	est. err($^\circ$)	5.7446 \pm 0.6879	5.7344 \pm 0.6870	5.6831 \pm 0.6793	5.6600 \pm 0.6536	5.7617 \pm 0.7506	34.1559 \pm 0.3833
	CPU time(s)	1.0918 \pm 0.1460	1.9741 \pm 0.3063	40.3212 \pm 0.7393	13.0203 \pm 1.5725	0.5475 \pm 0.1064	-
(ii)	est. err($^\circ$)	3.7542 \pm 0.4714	3.7569 \pm 0.4775	3.7373 \pm 0.4825	3.7311 \pm 0.4825	3.7350 \pm 0.4738	13.0605 \pm 0.2451
	CPU time(s)	1.0172 \pm 0.1194	1.9016 \pm 0.2039	169.6357 \pm 13.8678	12.5140 \pm 1.3909	0.5126 \pm 0.0828	-

with $H = \sigma I_{3 \times 3}$ and $\sigma = 1 \text{ deg}/\sqrt{s}$. The vector measurement errors follow the Gaussian distribution with zero mean and a covariance that varies by each example. For all examples, the simulation time is $T = 60s$ and the time step is $h = 0.02s$. The SVD method is utilized to estimate the attitude directly from vector measurements and calculate the measurement error. For each case, 50 Monte Carlo simulations (with respect to the random noise) are carried out. All simulations are conducted on a computer owning a 6-core Intel i7-9750H 2.6Ghz CPU, and 16G RAM.

Note that the two MFD-based Bayesian filters in [33] and [37] can not directly deal with common vector measurement errors characterized by Gaussian distributions. To compare the four filters, we use a method presented in [42] to approximate the directional distribution of vector measurements with Gaussian noise. For a random vector $x \in \mathbb{R}^3$ characterized by $x \sim \mathcal{N}(\mu, k^2 I_3)$, the possibility distribution density of $x_1 = x/\|x\|$ is given by

$$p(x_1) = \frac{\kappa}{4\pi \sinh \kappa} \exp(\kappa \mu_1 x_1), \quad (67)$$

where $\kappa = \|\mu\|^2/k^2$ and $\mu_1 = \mu/\|\mu\|$. For a more general case with $x \sim \mathcal{N}(\mu, \Sigma)$, κ is given by $3\|\mu\|^2/\text{tr}(\Sigma)$ to approximate the average dispersion characteristic of the directional distribution of x .

A. Small initial errors

In this subsection, measurement noises are chosen to be isotropic with $G_k^i = \sigma_m^2 I_3$ and $\sigma_m \in \mathbb{R}$. Two different levels of covariance are tested: (i) $\sigma_m = 0.24$; (ii) $\sigma_m = 0.04$. The initial parameter of the four filters with MFDs is $F_0 = 10 \exp(\pi e_1^\wedge/18)$, implying that the initial attitude information has a small error and high confidence. For the IEKF method, the corresponding initial attitude is $R_0 = \exp(\pi e_1^\wedge/18)$ with a covariance matrix $P_0 = \text{diag}[1/(s_2 + s_3), 1/(s_1 + s_3), 1/(s_1 + s_2)] = 0.05 I_3$, where s_i for $i \in \{1, 2, 3\}$ is the proper singular value of F_0 . The results are provided in Table III for comparison. The CPU time of one simulation is also averaged across all simulations. The attitude error at the k -th step of the i -th simulation is defined as $E_k^i = \|\log(\hat{R}_k^i R_k)^\vee\|$, where \hat{R}_k^i is the attitude estimate at the k -th step in the i -th simulation and R_k is the true attitude at the k -th step. The average attitude error and the standard deviation are defined, respectively, as

$$AE = \frac{h}{MT} \sum_{i=1}^M \sum_{k=1}^{T/h} E_k^i,$$

$$SD = \sqrt{\frac{1}{M-1} \sum_{i=1}^M \left(\frac{h}{T} \sum_{k=1}^{T/h} E_k^i - AE \right)^2}.$$

The results show that the accuracy and convergence rates of these five filters are almost identical. These results corroborate the analyses presented in Section III for a small initial error, in which the differences in κ_{MFD}^+ and κ_{CGD}^+ , and in $\bar{\theta}_{MFD}^+$ and $\bar{\theta}_{CGD}^+$ are minor since the mean attitudes of the prior and the likelihood distributions are almost identical. However, it is noteworthy that the average time consumption of the two proposed filters is only $1/20 \sim 1/100$ of BF-MFD and $1/5 \sim 1/10$ of BF-AMFD.

B. Large initial errors

This subsection considers three cases of measurement noises as (i) $G_k^i = 0.24 I_3$, $F_0 = 10^{-3} \exp(\pi e_1^\wedge)$; (ii) $G_k^i = 0.04 I_3$; (iii) $G_k^i = \text{diag}[0.3 \ 0.01 \ 0.01]$. The first two cases are chosen to be isotropic while the third case is chosen to be non-isotropic. The initial parameter of for the four MFD-based filters is

$$F_0 = \exp(\pi e_1^\wedge), \quad (68)$$

which implies that the initial estimate rotates 180° around e_1 compared to the true initial attitude and the initial uncertainties are large. The corresponding initial parameters are set as $R_0 = \exp(\pi e_1^\wedge)$ and $P_0 = 0.5 I_3$. The results are provided in Table IV and Fig. 5.

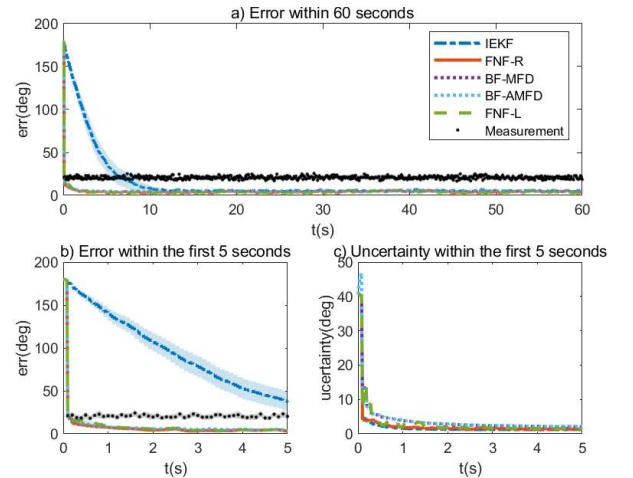


Fig. 5. Average error for the case of large initial errors with non-isotropic measurement errors. The shadow represents an envelope of 95% confidence. The attitude uncertainty is calculated as the square root of the first diagonal term of the attitude covariance matrix in the inertial frame as [36].

As shown in Fig. 5, the two proposed filters achieve, in cases i) and ii), almost identical estimation accuracy and convergence rate with BF-MFD and BF-AMFD, and, in case

TABLE IV
AE (\pm SD) AND TIME CONSUMPTION: LARGE INITIAL ERRORS

Measurement Model		FNF-R	FNF-L	BF-MFD	BF-AMFD	IEKF	Mea
(i)	est. err($^\circ$)	6.0655 \pm 0.7111	6.0835 \pm 0.7117	6.0144 \pm 0.6269	5.9955 \pm 0.5996	18.4045 \pm 10.0358	34.1242 \pm 0.3413
	CPU time(s)	1.3028 \pm 0.5569	2.3086 \pm 0.5107	43.5268 \pm 5.7680	14.0640 \pm 1.8289	0.6165 \pm 0.1707	-
(ii)	est. err($^\circ$)	4.1770 \pm 0.2373	4.1782 \pm 0.2350	4.1735 \pm 0.2237	4.1679 \pm 0.2219	17.9557 \pm 8.5424	13.0266 \pm 0.1162
	CPU time(s)	1.6769 \pm 0.4629	2.9920 \pm 0.5942	236.3250 \pm 23.9040	17.2814 \pm 2.3391	0.7756 \pm 0.1599	-
(iii)	est. err($^\circ$)	4.4662 \pm 0.2905	4.6372 \pm 0.3120	5.1864 \pm 0.3945	5.1754 \pm 0.3878	13.8843 \pm 5.0385	20.6025 \pm 0.2002
	CPU time(s)	1.6159 \pm 0.3840	2.9516 \pm 0.6162	56.7839 \pm 6.6287	18.1293 \pm 2.0038	0.8394 \pm 0.2066	-

iii), better estimation accuracy than BF-MFD and BF-AMFD, which cannot appropriately handle vector measurements with non-isotropic Gaussian noises. All MFD-based filters are much more accurate than IEKF in all three cases. More importantly, both proposed filters consume significantly less time than BF-MFD and BF-AMFD, which is shown in Fig. 6. The two proposed filters consume slightly more time than (approximately 2 ~ 3 times of) IEKF due to the involvement of matrix inversion in calculating the prior distribution, and much less time than BF-MFD and BF-AMFD (only 1/20 ~ 1/100 of BF-MFD and 1/5 ~ 1/10 of BF-AMFD) due to skipping the step of solving complex nonlinear equations in the moment matching as needed by BF-MFD and BF-AMFD. When comparing the results of cases (i) and (ii), it can be seen that a larger initial and measurement uncertainty leads to a slightly greater loss of accuracy for the FNF-R than for the BF-MFD and BF-AMFD. More specifically, accuracy loss increases from 1% for case(ii) and 2% for case (i), which is, unless extremely high estimation accuracy is required, insignificant in the presence of remarkable computational speed.

In Section III, we prove that the uncertainty of MFD-based Bayesian filters (measured by $1/\kappa^+$) is correlated with $\Delta\bar{\theta}$, while the uncertainty of filters with CGDs is independent of the mean angle. Therefore, in Fig. 5, the uncertainties of the four filters with MFDs decrease in a manner compatible with estimation errors, while the uncertainty of IEKF decreases rapidly even if the estimation error is still large. Additionally, the fast convergence of the errors of four MFD-based filters also corroborates the analysis in Section III. The filter with MFDs always filters out wrong information with low confidence faster than IEKF. These simulations show that even if linearized error systems are introduced to construct FNF-R and FNF-L, the two proposed filters still inherit the nonlinear filtering mechanism and, therefore, advantages discussed in Section III.

C. Direct attitude measurements with non-isotropic noise

Finally, we test cases of direct attitude measurements with non-isotropic noise. The direct attitude measurement model for the four filters with MFDs is given by

$$R_k^m = R_k \delta R, \quad \delta R \sim \mathcal{M}(N^m), \quad (69)$$

where $N^m \in \mathbb{R}^{3 \times 3}$ and $(N^m)^T = N^m$. The corresponding attitude measurement model for IEKF is given by

$$R_k^m = R_k \exp(\xi^\wedge), \quad \xi \sim \mathcal{N}(0, P^m). \quad (70)$$

All five filters will be tested with noisy measurements generated by (69) and (70), respectively. The measurement

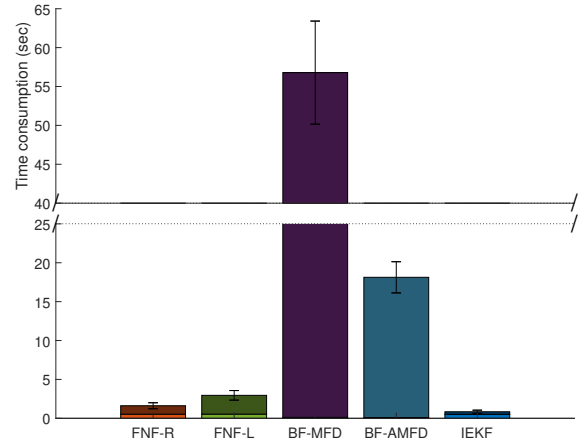


Fig. 6. Time consumption: large initial error with non-isotropic measurement error. For each bar, the darker part on the top represents the time consumption of the prior for the proposed filters or propagation for BF-MFD and IEKF, and the lighter part on the bottom represents the time consumption of the likelihood and the posterior for the proposed filters or the measurement update for BF-MFD and IEKF.

noises are set as: (i) $N^m = \text{diag}[100, 0, 0]$; (ii) $P^m = \text{diag}[10, 0.01, 0.01]$. The parameters P^m and N^m are chosen to be similar and correspond to the case that the rotation about the b_1 axis of \mathcal{F}_B is completely unknown. The rest parameter settings are the same as Section VI-A. The results are summarised in Table V and Fig. 7.

The two proposed filters maintain almost the same estimation accuracy as, and have significantly faster computation speed than BF-MFD and BF-AMFD. All four MFD-based filters achieve smaller steady-state errors compared to IEKF. This indicates that although FNF-R and FNF-L utilize the linearized error systems, they still perform much better than IEKF when dealing with large measurement uncertainty.

VII. CONCLUSION

This paper addressed the fast nonlinear filtering problem with MFDs on $SO(3)$. Two key properties associated with MFD-based attitude filters are revealed by analyzing the evolution of the distributions on $SO(3)$ along Bayes' rule: (i) the difference in mean attitudes of the prior and the likelihood distributions influence the uncertainty of the posterior distribution for rotations around a specific axis; (ii) MFD-based filters can filter out wrong information with low confidence faster than filters with CGDs. This finding is based on analytic expressions instead of a limited number

TABLE V
AE (\pm SD) AND TIME CONSUMPTION: DIRECT ATTITUDE MEASUREMENTS WITH NON-ISOTROPIC NOISE

Measurement Model		FNF-R	FNF-L	BF-MFD	BF-AMFD	IEKF	Mea
(i)	est. err($^\circ$)	3.9214 \pm 0.2150	4.0539 \pm 0.2390	3.8478 \pm 0.2035	3.8447 \pm 0.2021	4.666 \pm 0.3946	90.6634 \pm 0.9837
	CPU time(s)	0.7065 \pm 0.0838	1.5216 \pm 0.1374	154.9268 \pm 10.4637	11.6526 \pm 0.9604	0.6301 \pm 0.1936	-
(ii)	est. err($^\circ$)	3.3934 \pm 0.1292	3.4862 \pm 0.1306	3.3592 \pm 0.1246	3.3546 \pm 0.1244	3.7566 \pm 0.1677	90.9054 \pm 0.7501
	CPU time(s)	0.7306 \pm 0.0799	1.5648 \pm 0.1418	158.9332 \pm 11.1592	11.9009 \pm 1.1125	0.5766 \pm 0.0851	-

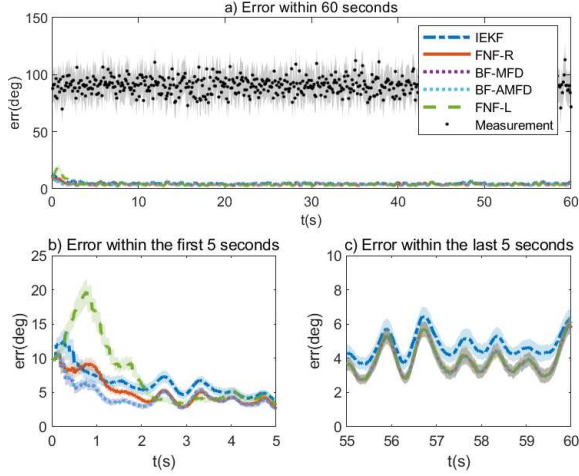


Fig. 7. Average error for the case of direct attitude measurements with non-isotropic noise: $N^m = \text{diag}[100, 0, 0]$.

of numerical examples or intuitive inferences. Therefore, it underpins the general validity and advantage of attitude filters with MFDs for estimation on $SO(3)$.

Two filters with MFDs are thereby proposed, and they retain the aforementioned properties but reduce the computational burden by a significant amount compared to previous MFD-based attitude filters. The proposed filters represent the attitude uncertainty by the left- and right-invariant errors characterized by MFDs respectively. Moreover, the filter with right-invariant error is proved to be almost-global exponentially stable for the single-axis rotation. The filter with right-invariant errors performs as well as the Bayesian filter with MFDs presented in [33] in challenging simulation examples but consumes much less computation time (about $1/5 \sim 1/100$ of previous MFD-based attitude filters). The filter with left-invariant errors is slightly less accurate than the previous Bayesian filter with MFDs, but still significantly better in terms of accuracy than the well-established IEKF in challenging circumstances. Therefore, the two proposed filters are efficient alternatives to the existing Bayesian filters with MFDs and IEKF for the attitude estimation requiring high computation efficiency.

APPENDIX A

The proof is based on mathematical induction. Assume that the posterior estimates at t_{k-1} are $\hat{R}_{k-1} = \exp(\hat{\theta}_{k-1} b_3)$, $N_{k-1} = \text{diag}[\kappa_{k-1}, \kappa_{k-1}, \kappa_{k-1}^*]$. The assumption is clearly valid at $t_1 = 1$. For $k > 1$, the prior

estimates provided by Algorithm 1 are

$$\begin{aligned}\hat{R}_{k|k-1} &= \hat{R}_{k-1} \exp(\tilde{w}_k b_3) = \exp\left[\left(\hat{\theta}_{k-1} + \tilde{w}_k h\right) b_3\right], \\ P_{k|k-1} &= P_{k-1} + \hat{R}_{k-1} Q_k \left(\hat{R}_{k-1}\right)^T \\ &= \text{diag}\left[\frac{1}{\kappa_{k-1} + \kappa_{k-1}^*}, \frac{1}{\kappa_{k-1} + \kappa_{k-1}^*}, \frac{1}{2\kappa_{k-1}}\right] + Q_k,\end{aligned}$$

and $N_{k|k-1}$ can then be derived by (31) as

$$N_{k|k-1} = \text{diag}[\kappa_{k|k-1}, \kappa_{k|k-1}, \kappa_{k|k-1}^*],$$

where

$$\begin{aligned}\kappa_{k|k-1} &= \frac{\kappa_{k-1}}{1 + 2\kappa_{k-1}\sigma_k}, \\ \kappa_{k|k-1}^* &= \frac{\kappa_{k-1} + \kappa_{k-1}^*}{1 + \sigma_k(\kappa_{k-1}^+ + \kappa_{k-1}^*)} - \frac{\kappa_{k-1}^+}{1 + 2\kappa_{k-1}^+\sigma_k}.\end{aligned}$$

For measurement update, F_k is calculated as

$$\begin{aligned}F_k &= N_k^m R_k^m + N_{k|k-1} \hat{R}_{k|k-1} \\ &= N_k^m \exp(\theta_k^m b_3) + N_{k|k-1} \exp(\hat{\theta}_{k|k-1} b_3) \\ &= \begin{bmatrix} \kappa_k^m \cos \theta_k^m & -\kappa_k^m \sin \theta_k^m \\ \kappa_k^m \sin \theta_k^m & \kappa_k^m \cos \theta_k^m \\ & & \kappa_k^{m*} \end{bmatrix} + \\ &\quad \begin{bmatrix} \kappa_{k|k-1} \cos \hat{\theta}_{k|k-1} & -\kappa_{k|k-1} \sin \hat{\theta}_{k|k-1} \\ \kappa_{k|k-1} \sin \hat{\theta}_{k|k-1} & \kappa_{k|k-1} \cos \hat{\theta}_{k|k-1} \\ & & \kappa_{k|k-1}^* \end{bmatrix}.\end{aligned}$$

Denote by $\Delta\theta_{k|k-1} = \theta_k^m - \theta_{k|k-1}$, and we have

$$\begin{aligned}&\kappa_k^m \cos \theta_k^m + \kappa_{k|k-1} \cos \hat{\theta}_{k|k-1} \\ &= \kappa_k^m \cos(\hat{\theta}_{k|k-1} + \Delta\theta_{k|k-1}) + \kappa_{k|k-1} \cos \hat{\theta}_{k|k-1} \\ &= (\kappa_{k|k-1} + \kappa_k^m \cos \Delta\theta_{k|k-1}) \cos \hat{\theta}_{k|k-1} - \kappa_k^m \sin \Delta\theta_{k|k-1} \sin \hat{\theta}_{k|k-1} \\ &= \kappa_k \cos(\hat{\theta}_{k|k-1} + \Delta\hat{\theta}_k) \\ &\kappa_k^m \sin \theta_k + \kappa_{k|k-1} \sin \hat{\theta}_{k|k-1} \\ &= \kappa_k^m \sin(\hat{\theta}_{k|k-1} + \Delta\theta_{k|k-1}) + \kappa_{k|k-1} \sin \hat{\theta}_{k|k-1} \\ &= (\kappa_{k|k-1} + \kappa_k^m \cos \Delta\theta_{k|k-1}) \sin \hat{\theta}_{k|k-1} + \kappa_k^m \sin \Delta\theta_{k|k-1} \cos \hat{\theta}_{k|k-1} \\ &= \kappa_k \sin(\hat{\theta}_{k|k-1} + \Delta\hat{\theta}_k),\end{aligned}$$

where

$$\begin{aligned}\kappa_k &= \sqrt{(\kappa_{k|k-1})^2 + (\kappa_k^m)^2 + 2\kappa_{k|k-1}\kappa_k^m \cos(\Delta\theta_k)}, \\ \Delta\hat{\theta}_k &= \text{sign}(\Delta\theta_k) \arccos\left(\frac{\kappa_{k|k-1} + \kappa_k^m \cos(\Delta\theta_k)}{\kappa_k}\right).\end{aligned}$$

Then, F_k can be rewritten as

$$F_k = \begin{bmatrix} \kappa_k I_2 & \\ & \kappa_k^{m*} + \kappa_{k|k-1}^* \end{bmatrix} \exp \left[\left(\hat{\theta}_{k|k-1} + \Delta \hat{\theta}_k \right) b_3^\wedge \right],$$

equivalent to the proper left polar decomposition of F_k . Thus, the posterior estimates are given by

$$N_k = \text{diag}[\kappa_k, \kappa_k^{m*} + \kappa_{k|k-1}^*],$$

$$\hat{R}_k = \exp \left[\left(\hat{\theta}_{k|k-1} + \Delta \hat{\theta}_k \right) b_3^\wedge \right],$$

which, under the induction assumption, preserves the forms of the diagonal matrix and the uniaxial rotation, respectively. By the mathematical induction, Theorem V.1 is valid for all positive integers k .

APPENDIX B

We first prove the monotonicity of V_k . Since the angular velocity measurements are noise-free, we have $\Delta \theta_{k|k-1} = \theta_k - \hat{\theta}_{k|k-1} = \Delta \theta_{k-1} = \theta_k - \hat{\theta}_{k-1}$, and thus

$$\frac{V_{k|k-1}}{V_{k-1}} = \frac{\kappa_{k|k-1}}{\kappa_{k-1}} = \frac{1}{1 + 2\kappa_{k-1}\sigma_k} < 1.$$

Defining an intermediate variable $k = \kappa_k^m / \kappa_{k|k-1}$, there is

$$\frac{V_k}{V_{k|k-1}} = \frac{\kappa_k \left[1 - \cos(\theta_k - \hat{\theta}_k) \right]}{\kappa_{k|k-1} \left[1 - \cos(\Delta \theta_{k|k-1}) \right]} = \frac{1 - \cos(\Delta \theta_{k|k-1} - \Delta \hat{\theta}_k)}{\sqrt{1 + k^2 + 2k \cos(\Delta \theta_{k|k-1})} \frac{1 - \cos(\Delta \theta_{k|k-1})}{1 - \cos(\Delta \theta_{k|k-1})}},$$

where $\Delta \hat{\theta}_k = \hat{\theta}_{k|k-1} - \hat{\theta}_k$. Because the noise-free measurement $R_k^m = R_k$, we have $\theta_k^m - \hat{\theta}_{k|k-1} = \Delta \theta_{k|k-1}$, and $\cos(\Delta \hat{\theta}_k)$ as well as $\sin(\Delta \hat{\theta}_k)$ can be rewritten as

$$\begin{aligned} & \cos \left[\text{sign}(\Delta \theta_{k|k-1}) \arccos \left(\frac{\kappa_{k|k-1} + \kappa_k^m \cos(\Delta \theta_{k|k-1})}{\kappa_k} \right) \right] \\ &= \frac{\kappa_{k|k-1} + \kappa_k^m \cos(\Delta \theta_k)}{\kappa_k} = \frac{1 + k \cos(\Delta \theta_{k|k-1})}{\sqrt{1 + k^2 + 2k \cos(\Delta \theta_{k|k-1})}}, \\ & \sin \left[\text{sign}(\Delta \theta_{k|k-1}) \arccos \left(\frac{\kappa_{k|k-1} + \kappa_k^m \cos(\Delta \theta_{k|k-1})}{\kappa_k} \right) \right] \\ &= \frac{k \sin \Delta \theta_{k|k-1}}{\sqrt{1 + k^2 + 2k \cos(\Delta \theta_{k|k-1})}}. \end{aligned}$$

Substituting $\cos(\Delta \hat{\theta}_k)$ and $\sin(\Delta \hat{\theta}_k)$ into $\cos(\Delta \theta_{k|k-1} - \Delta \hat{\theta}_k)$, we have

$$\begin{aligned} & \cos(\Delta \theta_{k|k-1} - \Delta \hat{\theta}_k) = \cos \Delta \theta_{k|k-1} \cos \Delta \hat{\theta}_k + \sin \Delta \theta_{k|k-1} \sin \Delta \hat{\theta}_k \\ &= \frac{\cos \Delta \theta_{k|k-1} + k \cos^2(\Delta \theta_{k|k-1})}{\sqrt{1 + k^2 + 2k \cos(\Delta \theta_{k|k-1})}} + \\ & \quad \frac{k \sin^2 \Delta \theta_{k|k-1}}{\sqrt{1 + k^2 + 2k \cos(\Delta \theta_{k|k-1})}} \\ &= \frac{\cos \Delta \theta_{k|k-1} + k}{\sqrt{1 + k^2 + 2k \cos(\Delta \theta_{k|k-1})}}. \end{aligned}$$

Substituting into $V_k/V_{k|k-1}$, there is

$$\begin{aligned} \frac{V_k}{V_{k|k-1}} &= \frac{\sqrt{1 + k^2 + 2k \cos(\Delta \theta_{k|k-1})} - k - \cos \Delta \theta_{k|k-1}}{1 - \cos(\Delta \theta_{k|k-1})} \\ &\leq \frac{1 + k - k - \cos \Delta \theta_{k|k-1}}{1 - \cos \Delta \theta_{k|k-1}} = 1, \end{aligned}$$

where the equality holds if and only if $\Delta \theta_{k|k-1} = 0$, i.e., the error converges to zero. Thus, we have

$$V_k \leq V_{k|k-1} = \frac{V_{k-1}}{1 + 2\kappa_{k-1}\sigma_k} < V_{k-1}. \quad (\text{B3})$$

Then, we consider the boundedness of V_k . Using (B1), $\cos(\theta_k - \hat{\theta}_k) / \cos(\theta_k - \hat{\theta}_{k|k-1})$ can be rewritten as

$$\frac{1 + k / \cos(\Delta \theta_{k|k-1})}{\sqrt{1 + k^2 + 2k \cos(\Delta \theta_{k|k-1})}} \geq 1, \quad (\text{B4})$$

where the equality holds if and only if $\Delta \theta_{k|k-1} = 0$. The equation (B4) implies that the estimation error monotonically decreases as k increases, i.e.,

$$1 - \cos(\theta_k - \hat{\theta}_k) < 1 - \cos(\theta_k - \hat{\theta}_{k|k-1}) = 1 - \cos(\theta_{k-1} - \hat{\theta}_{k-1}). \quad (\text{B5})$$

At each step, we have

$$0 \leq \kappa_{k|k-1} = \frac{\kappa_{k-1}}{1 + 2\kappa_{k-1}\sigma_k} < \frac{1}{2\alpha_1}.$$

View κ_k as a function with respect to $\kappa_{k|k-1}$, κ_k^m and $\cos \Delta \theta_{k|k-1}$, and there is, for all $k > 0$,

$$\begin{aligned} & \max \left\{ \kappa_k^m, \sqrt{\frac{1}{4\alpha_1^2} + (\kappa_k^m)^2 + \frac{\kappa_k^m}{\alpha_1} \cos \Delta \theta_{k|k-1}} \right\} \geq \kappa_k \\ & \geq \begin{cases} \kappa_k^m, & 1 \geq \cos \Delta \theta_{k|k-1} > 0, \\ \kappa_k^m |\sin \Delta \theta_{k|k-1}|, & -1 < \cos \Delta \theta_{k|k-1} \leq 0. \end{cases} \end{aligned}$$

Since $\|R_0 - \hat{R}_0\|_F \leq 4 - \epsilon$, i.e., $\cos(\Delta \theta_0) > -1 + \epsilon/2$, and estimation error monotonically decreases as (B5), we have

$$\kappa_k \geq \kappa_k^m \sqrt{1 - \cos^2 \Delta \theta_{k|k-1}} \geq \beta_1 \sqrt{\epsilon - \frac{\epsilon^2}{4}}$$

when $-1 < \cos \Delta \theta_{k|k-1} \leq 0$, and

$$\kappa_k \geq \kappa_k^m \geq \beta_1$$

when $0 < \cos \theta_{k|k-1} \leq 1$. Thus, a lower bound of V_k is given by

$$V_k \geq \beta_1 \sqrt{\epsilon - \frac{\epsilon^2}{4}} (1 - \cos \Delta \theta_k). \quad (\text{B6})$$

For the upper bound, we have

$$\begin{aligned} & \sqrt{\frac{1}{4\alpha_1^2} + (\kappa_k^m)^2 + \frac{\kappa_k^m}{\alpha_1} \cos \Delta \theta_{k|k-1}} \leq \sqrt{\left(\frac{1}{2\alpha_1} - \kappa_k^m \right)^2 + \frac{\kappa_k^m \epsilon}{2\alpha_1}} \\ & \leq \max \left\{ \sqrt{\left(\frac{1}{2\alpha_1} - \beta_1 \right)^2 + \frac{\beta_1 \epsilon}{2\alpha_1}}, \sqrt{\left(\frac{1}{2\alpha_1} - \beta_2 \right)^2 + \frac{\beta_2 \epsilon}{2\alpha_1}} \right\} \end{aligned} \quad (\text{B1})$$

Thus, V_k is bounded by

$$\gamma_1 (1 - \cos \Delta \theta_k) \leq V_k \leq \gamma_2 (1 - \cos \Delta \theta_k), \quad (\text{B7})$$

where $\gamma_1 = \beta_1 \sqrt{\epsilon - \epsilon^2/4}$ and

$$\gamma_2 = \max \left\{ \beta_2, \sqrt{\left(\frac{1}{2\alpha_1} - \beta_1\right)^2 + \frac{\beta_1\epsilon}{2\alpha_1}}, \sqrt{\left(\frac{1}{2\alpha_1} - \beta_2\right)^2 + \frac{\beta_2\epsilon}{2\alpha_1}} \right\}.$$

Finally, we prove that the estimation error decreases exponentially. Using (B3), we have

$$V_k \leq \frac{V_{k-1}}{1 + 2\kappa_{k-1}\sigma_k} \leq \frac{V_{k-1}}{1 + 2\alpha_2\beta_1\sqrt{\epsilon - \frac{\epsilon^2}{4}}},$$

and thus

$$V_k \leq \frac{V_0}{\left(1 + 2\alpha_2\beta_1\sqrt{\epsilon - \frac{\epsilon^2}{4}}\right)^k}. \quad (\text{B8})$$

According to (63), V_k can be rewritten as $V_k = (\kappa_k/2)\|R_k - \hat{R}_k\|_F$ and (B8) can be extended to

$$\begin{aligned} \|R_k - \hat{R}_k\|_F &\leq \frac{\kappa_0}{\kappa_k \left(1 + 2\alpha_2\beta_1\sqrt{\epsilon - \frac{\epsilon^2}{4}}\right)^k} \|R_0 - \hat{R}_0\|_F \\ &\leq \frac{\kappa_0}{\gamma_2 \left(1 + 2\alpha_2\beta_1\sqrt{\epsilon - \frac{\epsilon^2}{4}}\right)^k} \|R_0 - \hat{R}_0\|_F, \end{aligned}$$

which verifies (64).

REFERENCES

- [1] R. Mahony, T. Hamel, and J.-M. Pflimlin, "Nonlinear complementary filters on the special orthogonal group," *IEEE Transactions on automatic control*, vol. 53, no. 5, pp. 1203–1218, 2008.
- [2] D. E. Zlotnik and J. R. Forbes, "Higher order nonlinear complementary filtering on lie groups," *IEEE Transactions on Automatic Control*, vol. 64, no. 5, pp. 1772–1783, 2018.
- [3] T.-H. Wu, E. Kaufman, and T. Lee, "Globally asymptotically stable attitude observer on $so(3)$," in *2015 54th IEEE Conference on Decision and Control (CDC)*, pp. 2164–2168, IEEE, 2015.
- [4] S. Berkane, A. Abdessameud, and A. Tayebi, "Hybrid global exponential stabilization on $so(3)$," *Automatica*, vol. 81, pp. 279–285, 2017.
- [5] S. Berkane, A. Abdessameud, and A. Tayebi, "Hybrid attitude and gyro-bias observer design on $so(3)$," *IEEE Transactions on Automatic Control*, vol. 62, no. 11, pp. 6044–6050, 2017.
- [6] M. Wang and A. Tayebi, "Hybrid nonlinear observers for inertial navigation using landmark measurements," *IEEE Transactions on Automatic Control*, vol. 65, no. 12, pp. 5173–5188, 2020.
- [7] M. Wang and A. Tayebi, "Nonlinear attitude estimation using intermittent and multirate vector measurements," *IEEE Transactions on Automatic Control*, vol. 69, no. 8, pp. 5231–5245, 2023.
- [8] E. Lefferts, F. Markley, and M. Shuster, "Kalman Filtering for Spacecraft Attitude Estimation," *Journal of Guidance, Control, and Dynamics*, vol. 5, pp. 417–429, Sept. 1982.
- [9] F. L. Markley, "Attitude error representations for kalman filtering," *Journal of guidance, control, and dynamics*, vol. 26, no. 2, pp. 311–317, 2003.
- [10] A. Barrau and S. Bonnabel, "Intrinsic Filtering on Lie Groups With Applications to Attitude Estimation," *IEEE Transactions on Automatic Control*, vol. 60, pp. 436–449, Feb. 2015.
- [11] A. Barrau and S. Bonnabel, "The Invariant Extended Kalman Filter as a Stable Observer," *IEEE Transactions on Automatic Control*, vol. 62, pp. 1797–1812, Apr. 2017.
- [12] A. Barrau and S. Bonnabel, "Stochastic observers on Lie groups: A tutorial," in *2018 IEEE Conference on Decision and Control (CDC)*, pp. 1264–1269, IEEE, 2018.
- [13] A. Barrau and S. Bonnabel, "The invariant extended kalman filter as a stable observer," *IEEE Transactions on Automatic Control*, vol. 62, no. 4, pp. 1797–1812, 2016.
- [14] A. Barrau and S. Bonnabel, "Extended Kalman Filtering With Nonlinear Equality Constraints: A Geometric Approach," *IEEE Transactions on Automatic Control*, vol. 65, pp. 2325–2338, June 2020.
- [15] A. Barrau and S. Bonnabel, "The geometry of navigation problems," *IEEE Transactions on Automatic Control*, vol. 68, no. 2, pp. 689–704, 2022.
- [16] H. Gui and A. H. J. de Ruiter, "Quaternion Invariant Extended Kalman Filtering for Spacecraft Attitude Estimation," *Journal of Guidance, Control, and Dynamics*, vol. 41, pp. 863–878, Apr. 2018.
- [17] A. Barrau and S. Bonnabel, "An EKF-SLAM algorithm with consistency properties," *arXiv preprint arXiv:1510.06263*, 2015.
- [18] C. Liu, C. Jiang, and H. Wang, "InGVIO: A Consistent Invariant Filter for Fast and High-Accuracy GNSS-Visual-Inertial Odometry," *IEEE Robotics and Automation Letters*, vol. 8, pp. 1850–1857, Mar. 2023.
- [19] Y. Song, Z. Zhang, J. Wu, Y. Wang, L. Zhao, and S. Huang, "A Right Invariant Extended Kalman Filter for Object Based SLAM," *IEEE Robotics and Automation Letters*, vol. 7, pp. 1316–1323, Apr. 2022.
- [20] G. S. Chirikjian, *Stochastic models, information theory, and Lie groups, volume 2: Analytic methods and modern applications*, vol. 2. Springer Science & Business Media, 2011.
- [21] A. Barrau and S. Bonnabel, "Invariant Kalman Filtering," *Annual Review of Control, Robotics, and Autonomous Systems*, vol. 1, pp. 237–257, May 2018.
- [22] Y. Wang and G. S. Chirikjian, "Error propagation on the Euclidean group with applications to manipulator kinematics," *IEEE Transactions on Robotics*, vol. 22, no. 4, pp. 591–602, 2006.
- [23] Y. Wang and G. S. Chirikjian, "Nonparametric second-order theory of error propagation on motion groups," *The International journal of robotics research*, vol. 27, no. 11–12, pp. 1258–1273, 2008.
- [24] K. C. Wolfe, M. Mashner, and G. S. Chirikjian, "Bayesian fusion on lie groups," *Journal of Algebraic Statistics*, vol. 2, no. 1, 2011.
- [25] G. Bourmaud, R. Mégret, M. Arnaudon, and A. Giremus, "Continuous-discrete extended kalman filter on matrix lie groups using concentrated gaussian distributions," *Journal of Mathematical Imaging and Vision*, vol. 51, pp. 209 – 228, 2014.
- [26] W. Wang and T. Lee, "Matrix Fisher–Gaussian distribution on $SO(3) \times \mathbb{R}^n$ and Bayesian attitude estimation," *IEEE Transactions on Automatic Control*, vol. 67, no. 5, pp. 2175–2191, 2021.
- [27] K. V. Mardia and P. E. Jupp, eds., *Directional Statistics*. Wiley Series in Probability and Statistics, Hoboken, NJ, USA: John Wiley & Sons, Inc., Jan. 1999.
- [28] C. Ley and T. Verdebout, *Modern Directional Statistics*. Chapman and Hall/CRC, 1 ed., Aug. 2017.
- [29] C. Ley and T. Verdebout, eds., *Applied Directional Statistics*. Boca Raton, FL: CRC Press, 2019.
- [30] T. D. Downs, "Orientation statistics," *Biometrika*, vol. 59, no. 3, pp. 665–676, 1972.
- [31] C. G. Khatri and K. V. Mardia, "The von Mises-Fisher Matrix Distribution in Orientation Statistics," *Journal of the Royal Statistical Society: Series B (Methodological)*, vol. 39, pp. 95–106, Sept. 1977.
- [32] C. Bingham, "An antipodally symmetric distribution on the sphere," *The Annals of Statistics*, pp. 1201–1225, 1974.
- [33] T. Lee, "Bayesian attitude estimation with the matrix Fisher distribution on $SO(3)$," *IEEE Transactions on Automatic Control*, vol. 63, no. 10, pp. 3377–3392, 2018.
- [34] G. Kurz, I. Gilitschenski, and U. D. Hanebeck, "Unscented von Mises–Fisher Filtering," *IEEE Signal Processing Letters*, vol. 23, pp. 463–467, Apr. 2016.
- [35] W. Wang and T. Lee, "Bingham-Gaussian Distribution on $S^3 \times \mathbb{R}^n$ for Unscented Attitude Estimation," in *2021 IEEE International Conference on Multisensor Fusion and Integration for Intelligent Systems (MFI)*, pp. 1–7, IEEE, 2021.
- [36] W. Wang and T. Lee, "Matrix Fisher-Gaussian distribution on $SO(3) \times \mathbb{R}^n$ for attitude estimation with a gyro bias," *arXiv preprint arXiv:2003.02180*, 2020.
- [37] T. Lee, "Bayesian Attitude Estimation with Approximate Matrix Fisher Distributions on $SO(3)$," in *2018 IEEE Conference on Decision and Control (CDC)*, (Miami Beach, FL), pp. 5319–5325, IEEE, Dec. 2018.
- [38] F. L. Markley, "Attitude determination using vector observations and the singular value decomposition," *Journal of the Astronautical Sciences*, vol. 36, no. 3, pp. 245–258, 1988.
- [39] G. S. Chirikjian, *Engineering Applications of Noncommutative Harmonic Analysis: With Emphasis on Rotation and Motion Groups*. CRC press, 2000.
- [40] R. A. Fisher, "Dispersion on a sphere," *Proceedings of the Royal Society of London. Series A. Mathematical and Physical Sciences*, vol. 217, no. 1130, pp. 295–305, 1953.

- [41] T. Lee, "Matrix Fisher distribution." Available: <https://github.com/fdcl-gwu/Matrix-Fisher-Distribution>, 2017. [Online].
- [42] J. J. Love and C. G. Constable, "Gaussian statistics for palaeomagnetic vectors," *Geophysical Journal International*, vol. 152, pp. 515–565, Mar. 2003.